Statistical Theory and Related Fields

ISSN: 2475-4269 (Print) 2475-4277 (Online) Journal homepage: www.tandfonline.com/journals/tstf20

Study and improvement of a multivariate covariance control chart based on the Sparse Group Lasso penalty

Jun Hu, Hongwei Li, Chunjie Wu & Jialin Wu

To cite this article: Jun Hu, Hongwei Li, Chunjie Wu & Jialin Wu (2026) Study and improvement of a multivariate covariance control chart based on the Sparse Group Lasso penalty, Statistical Theory and Related Fields, 10:1, 82-116, DOI: 10.1080/24754269.2025.2603538

To link to this article: https://doi.org/10.1080/24754269.2025.2603538

Published online: 22 Dec 2025.

STATISTICAL THEORY AND RELATED FIELDS
2026, VOL. 10, NO. 1, 82–116
https://doi.org/10.1080/24754269.2025.2603538

Study and improvement of a multivariate covariance control chart based on the Sparse Group Lasso penalty

Jun Hu[a], Hongwei Li[b], Chunjie Wu [b] and Jialin Wu[b]

[a]School of Mathematical Sciences, Shanghai Jiao Tong University, Shanghai, People's Republic of China; [b]School of Statistics and Data Science, Shanghai University of Finance and Economics, Shanghai, People's Republic of China

ABSTRACT

Traditional multivariate parametric control charts often perform inadequately in detecting shifts in the covariance matrix when the data deviate from normality. In this paper, we propose a multivariate nonparametric exponentially weighted moving average (SGLGEWMA) control chart, incorporating a Sparse Group Lasso penalty, which is capable of detecting shifts in the covariance matrix across a wide range of data types, including discrete, continuous, and mixed distributions. The proposed approach projects multivariate data into a Euclidean space and then computes an approximate Alt's likelihood ratio, regularized via the Sparse Group Lasso. The resulting EWMA statistic monitors process shifts. Monte Carlo simulations demonstrate that SGLGEWMA outperforms both the Lasso-based LGShewhart and the Ridge-based RGEWMA control charts under various distributions, with enhanced efficacy in high-dimensional scenarios. Sensitivity analyses are performed on the tuning parameters (λ_1, λ_2) and smoothing parameter ρ, to evaluate their impact on monitoring performance. Additionally, a simulation study and an illustrative example involving covariance monitoring in wafer semiconductor manufacturing are presented to demonstrate the practical application of the proposed chart. Empirical results confirm that the proposed control chart promptly identifies abnormal fluctuations and issues timely alerts, highlighting both its theoretical significance and practical utility.

ARTICLE HISTORY
Received 28 June 2025
Revised 21 October 2025
Accepted 9 December 2025

KEYWORDS
Covariance monitoring; nonparametric method; sparse group Lasso penalty; principal coordinate analysis; statistical process monitoring (SPM)

1. Introduction

1.1. Research background and significance

Statistical Process Monitoring (SPM) was originally developed to monitor industrial processes and ensure production quality. Over time, its application has been extended to diverse fields, including healthcare, chemical manufacturing, financial services, and environmental monitoring. A central tool in SPM is the Quality Control Chart (QCC), which integrates historical and real-time data to define upper and lower control limits. These limits are specifically designed to detect deviations from expected process behaviour and to signal potential anomalies that exceed predefined thresholds promptly.

CONTACT Chunjie Wu wumaths@mail.shufe.edu.cn School of Statistics and Data Science, Shanghai University of Finance and Economics, 777 Guoding Road, Yangpu District, Shanghai 200433, People's Republic of China

This article has been corrected with minor changes. These changes do not impact the academic content of the article.

With ongoing advances in industry and data science, modern manufacturing processes often generate complex and high-dimensional data. In recent years, numerous studies have demonstrated that joint monitoring approaches outperform univariate methods in such contexts. Traditional one-dimensional control charts, such as the Shewhart chart and the Exponentially Weighted Moving Average (EWMA) chart, are often inadequate to effectively monitor quality in production systems. These methods, particularly the average control chart and EWMA, struggle to capture the intricacies of real-world processes. In addition, many traditional control charts are developed under the assumption that the process data follow a multivariate normal distribution. However, this assumption frequently does not hold in practice, especially for high-dimensional processes. As dimensionality increases, the normality assumption becomes increasingly unrealistic, and parameter estimation within control charts becomes less reliable. This highlights the limitations of traditional methods under nonnormal conditions. Consequently, there is a pressing need to develop multivariate control charts that are robust to nonnormality, enabling more accurate and effective monitoring of modern production processes.

In real-world production processes, it is often necessary to monitor a large amount of multidimensional data, in which the mean vector μ and the covariance matrix Σ of the underlying distribution may change. Consequently, it is crucial to design appropriate monitoring schemes that can effectively track changes in both parameters. In many existing monitoring programs for the mean vector μ, researchers commonly assume that the covariance matrix Σ remains constant (for example, Σ is stable when μ changes). Under this assumption, monitoring μ becomes more reliable. However, if Σ itself is unstable, such an assumption may no longer hold, and any alarms triggered could be due to changes in Σ rather than genuine shifts in μ, thereby compromising the validity of the monitoring system. Therefore, effective monitoring of the covariance matrix Σ is essential to ensure an accurate interpretation of the variations of the process and to distinguish between changes in location and dispersion.

1.2. Literature review

For multivariate process monitoring, Hotelling (1947) initially introduced a control chart based on the Hotelling statistic T^2. However, subsequent studies revealed that applying univariate control chart techniques to monitor the T^2 statistic at each time point did not achieve the desired average run length (ARL) performance. To address this limitation, Woodall and Ncube (1985) proposed the Multivariate Cumulative Sum (MCUSUM) control chart, and Lowry et al. (1992) introduced the Multivariate Exponentially Weighted Moving Average (MEWMA) control chart.

Although these traditional multivariate control charts have been widely adopted, they typically rely on the assumption that the underlying process follows a multivariate normal distribution. In practice, however, this assumption may not hold, especially in complex or high-dimensional processes. Relying on such distributional assumptions can significantly affect the effectiveness of parameter monitoring. On the one hand, deviations from the normality assumption can cause the control chart's run length distribution to deviate from the expected value, making it difficult to accurately detect process shifts. On the other hand, test statistics derived under normality assumptions may lack sensitivity to shifts in nonnormal processes, potentially delaying or failing to issue timely out-of-control(OC) warnings.

The establishment of multivariate nonparametric control charts faces theoretical challenges. The core difficulty lies in the complexity of high-dimensional data structures, which hinders the straightforward extension of traditional univariate nonparametric concepts such as order, sign, and rank. Nevertheless, substantial progress has been made over the past decade, with notable approaches including data depth-based methods, robust rank-based estimators in vector spaces, and monitoring frameworks built upon nonparametric hypothesis testing. In the system of data depth methods, Liu (1995) introduced the Tukey depth function into the process monitoring, constructing a control chart capable of simultaneously tracking shifts in multivariate location and dispersion parameters, thereby eliminating reliance on the multivariate normality assumption inherent in traditional parametric methods. Based on this research, J. Li et al. (2013) proposed two innovative control charts, SS-CUSUM and DD-CUSUM, by innovatively integrating spatial symbols and data depth. These charts can efficiently detect shifts in location and anomalies in scale parameters, respectively, while maintaining distributional robustness.

Rank-based methods offer another promising direction. Zou et al. (2012) developed a nonparametric version of the multivariate EWMA control chart by leveraging ranks derived from Euclidean distance spaces. Through recursive updating of the rank-based covariance matrix, the proposed method significantly enhances sensitivity to small process shifts. Notably, the introduction of the concept of vector inverse rank provides a new theoretical tool for rank construction in the high-dimensional case.

The control charts mentioned above are mostly based on data depth and rank-based information to construct multivariate nonparametric control charts. Many multivariate nonparametric control charts use nonparametric tests to analyze process data. For instance, Mukherjee and Chakraborti (2012) combined the Wilcoxon rank-sum test with the Ansari-Bradley test to propose a Shewhart-type multivariate nonparametric control chart capable of simultaneously monitoring both the mean and covariance. Building on this, Chowdhury et al. (2014) developed a control chart based on the Cucconi two-sample test, replacing the original test combination with a more efficient statistic, thereby enhancing the overall monitoring performance. These control charts establish statistics through nonparametric tests, thereby avoiding poor control effects caused by parameter estimation in production processes with non-normal distributions. The above control charts can monitor process means, covariance matrices, or both means and covariance matrices separately. Here, we focus more on control chart schemes that monitor covariance matrices separately.

Since the transformation of the overall covariance matrix Σ is partially reflected in the sample covariance matrix S, researchers often construct monitoring statistics based on S. In some early studies, the determinant and trace of S were used as monitoring statistics. For example, Montgomery and Wadsworth (1972) used the determinant of S for monitoring, while Reynolds Jr and Cho (2006) used the trace of S to monitor variance shifts. However, this approach has certain limitations: if the structure of S changes but the determinant and trace remain unchanged, the shift cannot be detected.

Based on the progressive likelihood ratio test method, Alt (1984) proposed a generalized likelihood ratio (GLR) monitoring statistic for a single sample that does not have the above problem:

$$w_i = -(m-1)\left\{p + \ln\frac{|S_i|}{|\Sigma_0|} - \operatorname{tr}\left(\Sigma_0^{-1}S_i\right)\right\}, \tag{1}$$

where S_i is the $(p \times p)$ covariance matrix of the ith sample, m is the number of samples, p is the number of observed variables (sample dimension), and Σ_0 is the population covariance matrix when the process is in control (IC). When m is large, w_i is approximately distributed as $\chi^2_{p(p-1)}$. The advantage of the statistic w_i is that it can detect any shift in the covariance matrix.

In addition to the monitoring scheme proposed by Alt (1984), the following monitoring schemes are also classic and are often used as comparison schemes in many literatures: Yeh et al. (2005) separated the variance term and the covariance term, calculated the corresponding statistics separately, and took the maximum value as the final monitoring statistic, proposing the MaxMEWMV control chart; Huwang et al. (2007) extracted shift information from the covariance matrix based on its trace, proposing the MEWMS control chart and MEWMV control chart under conditions where the mean vector remains constant and changes, respectively; Hawkins and Maboudou-Tchao (2008) proposed the MEWMC control chart, building upon the ideas of Alt (1984) and Huwang et al. (2007). They assumed that Σ_0 is the identity matrix and ignored the constant term $m-1$ in Equation (1), resulting in the statistic

$$c_n = \mathrm{tr}\,(S_n) - \ln|S_n| - p, \tag{2}$$

where $S_0 = I_p$, $S_n = (1-\rho)S_{n-1} + \rho U_n U_n^\top (n \geq 1)$, and U_n is obtained by centralizing and standardizing the actual data X_n.

There are also some charts that can jointly monitor the mean and the variance. G. Zhang and Chang (2008) proposed a combined DEWMA-MEWMD (CDM) chart for monitoring the mean vector and variances in the variance-covariance matrix. Based on this, J. Zhang et al. (2010) proposed a new single control chart which integrates the EWMA procedure with the GLR test to jointly monitor the mean and variability of the multivariate process.

Around 2008, some researchers conducted research on the estimation of the covariance matrix sparsity. A representative example is the Graphical Lasso algorithm proposed by Friedman et al. (2008), which is used to obtain the sparsity estimation of the inverse covariance matrix based on the Lasso penalty:

$$\arg\max_{\Omega} \left\{\log|\Omega| - \mathrm{tr}(\Omega S) - \lambda\|\Omega\|_1\right\}. \tag{3}$$

The solution $\widehat{\Omega}$ to the above optimization problem is a sparse, full-rank estimate of the precision matrix Ω of the sample covariance matrix S, where the penalty term $\|\Omega\|_1$ is the L_1 norm of Ω. Different values of λ yield different degrees of sparsity for Ω. Using the Graphical Lasso algorithm, we obtain the estimate $\widehat{\Omega}$ of Ω, and thereby obtain the sparse, full-rank estimate $\widehat{S} = \widehat{\Omega}^{-1}$ of S.

In recent years, there have been some developments in the estimation of the sparsity of covariance matrices and precision matrices. Danaher et al. (2014) pointed out that the standard method for the above Gaussian graphical model assumes that each observation comes from the same distribution. When observations may correspond to multiple different categories, this assumption is unreasonable. They proposed an inverse covariance matrix sparsity estimation based on the Sparse Group Lasso penalty:

$$\arg\max_{\Omega} \left\{\log|\Omega| - \mathrm{tr}(\Omega S) - \lambda_1\|\Omega\|_1 - \lambda_2\|\Omega\|_2\right\}. \tag{4}$$

The improved Alternating Directions Method of Multipliers (ADMM) algorithm is used to solve the above optimization problem. The main difference between this algorithm and

the Graphical Lasso algorithm proposed by Friedman et al. (2008) is the addition of the L_2 norm of $\boldsymbol{\Omega}$. Compared to the Lasso penalty, the advantage of Sparse Group Lasso is that when estimating the sparsity matrix, it not only encourages group sparsity but also allows for intra-group sparsity. In high-dimensional data, the sparsity selection of Lasso may be affected by noise, leading to unstable selection, especially for highly correlated variables. Other Fused Lasso penalties (Hoefling, 2010) and Group Lasso penalties (Guo et al., 2011) are also discussed in the paper by Danaher et al. (2014).

Inspired by these studies, the idea of sparse estimation began to be introduced into covariance matrix monitoring. Some researchers believe that in actual data scenarios, it is unlikely that many terms in the covariance matrix $\boldsymbol{\Sigma}$ will shift simultaneously; rather, it is more likely that only a small number of terms will shift. However, even when the process is IC, the sample covariance matrix S may still have many nonzero terms. Some of these non-zero entries act as noise and interfere with monitoring. Furthermore, when the sample size n is smaller than the dimension p or under other conditions, S is singular and most of the eigenvalues of $\boldsymbol{\Sigma}$ are incorrectly estimated as zero. Similarly, the covariance matrix can be regularized by contracting it to a target structure to ensure that it is non-singular. Therefore, when monitoring the covariance matrix, one can first perform a sparse estimate of S to filter out noise and retain only information potentially related to the shift, followed by constructing the monitoring statistic. Yeh et al. (2012), J. Li et al. (2013), Maboudou-Tchao and Agboto (2013), and Maboudou-Tchao and Diawara (2013) have conducted some valuable work in this area.

The control charts for monitoring the covariance matrix mentioned above are all based on the assumption of a normal distribution. If the actual data distribution is approximately normal, these control charts exhibit good monitoring performance. Liang et al. (2019) pointed out that when the data distribution deviates significantly from the normal distribution, the monitoring effectiveness of many methods deteriorates. In recent years, researchers have proposed several nonparametric monitoring schemes. Ajadi et al. (2021) performed a logarithmic transformation on the main diagonal elements of the sample covariance matrix and constructed monitoring statistics based on this; Song et al. (2021) proposed an adaptive method for joint monitoring of the mean vector and covariance matrix of a binary process; Adegoke et al. (2022) adopted a projection method and sparse estimation ideas to propose a nonparametric monitoring scheme. For the latest research on covariance matrix monitoring, further reading is recommended in the research papers by Xu and Deng (2023) and Chakraborty and Finkelstein (2024).

1.3. Structure of the paper

In multivariate control charts, most studies are based on the assumption that the process distribution follows a multivariate normal distribution, that is, multivariate parametric control charts. However, in practical applications, this assumption often does not hold as the process distribution may not be normal or even continuous. Consequently, parameter estimates under the normal assumption can lead to poor control chart performance. For multivariate nonparametric control charts, improving methods for analyzing spatial information in historical data or establishing statistical measures can improve the performance of the control chart. Combining the data processing method using projections from Adegoke et al. (2022) and the method for estimating the sparsity of the covariance matrix based on the Sparse Group Lasso penalty from Danaher et al. (2014), we will establish an EWMA control chart based on the Euclidean space projection and the Sparse Group Lasso penalty likelihood ratio

to monitor the change of the covariance matrix. During the construction of the EWMA monitoring statistic, we have accounted for both the shift in the covariance term and the shift in the variance term.

There are two phases in statistical process monitoring: Phase I and Phase II. In Phase I, historical data are collected and control limits are derived. In Phase II, real-time data are monitored, and the control chart responds to potential OC signals. In our monitoring scheme, during Phase I, the IC data are projected into Euclidean space with a dimension less than or equal to the true dimension, and then the EWMA statistic is calculated based on the approximate Alt's likelihood ratio using the Sparse Group Lasso penalty. In Phase II, new observed data are projected onto the principal axes determined in Phase I, and the projected coordinate data are used to calculate the monitoring statistic. If the monitoring statistic exceeds the control limit, it indicates that the covariance has shifted.

After proposing the monitoring scheme, simulation testing and performance comparisons are conducted. The simulation testing process considers the influence of three factors: (1) sample dimension, (2) distribution of the monitored data, and (3) magnitude and type of shifts. It examines the impact of three different types of shifts on the control chart: variance shift, covariance shift, and simultaneous variance and covariance shift. In the simulation testing process, the proposed control chart is compared with two existing methods in terms of performance. The effectiveness of the control chart scheme in Phase II is typically measured by the ARL, defined as the average number of steps plotted on the chart before detecting an OC signal. The ARL for the IC and OC cases are denoted as ARL_0 and ARL_1, respectively. In this paper, the Monte Carlo simulation method will be used for the ARL calculation.

At the same time, a sensitivity analysis will be conducted on the control chart. It should be noted that the penalty term tuning parameters in the Sparse Group Lasso penalty likelihood ratio function and the smoothing parameter in the EWMA statistic also have a certain impact on the performance of the control chart. We will conduct sensitivity tests on these parameters. Then, implementation steps for the chart and examples of semiconductor grinding processes will be examined, and finally, a summary and outlook for multivariate nonparametric control charts will be provided.

The structure of this paper is as follows: Section 2 covers the theory of control charts, primarily introducing Euclidean space projection, the construction of statistical quantities, the determination of control limits, and a brief overview of related control charts; Section 3 focuses on statistical simulation, comparing the performance of control charts under three different shift conditions; Section 4 addresses sensitivity analysis, including the effects of penalty term tuning parameters and smoothing parameter on control chart performance; Section 5 analyzes the computational cost of the proposed chart; Section 6 presents case studies, which includes implementation steps and an example of a semiconductor grinding process; Section 7 summarizes the paper and provides prospects. The paper framework is shown in Figure 1.

2. The proposed monitoring scheme

2.1. Projection onto the same or lower dimensional Euclidean space

In this subsection, to fairly compare the monitoring effects of different control charts, we follow the settings used by Adegoke et al. (2022).

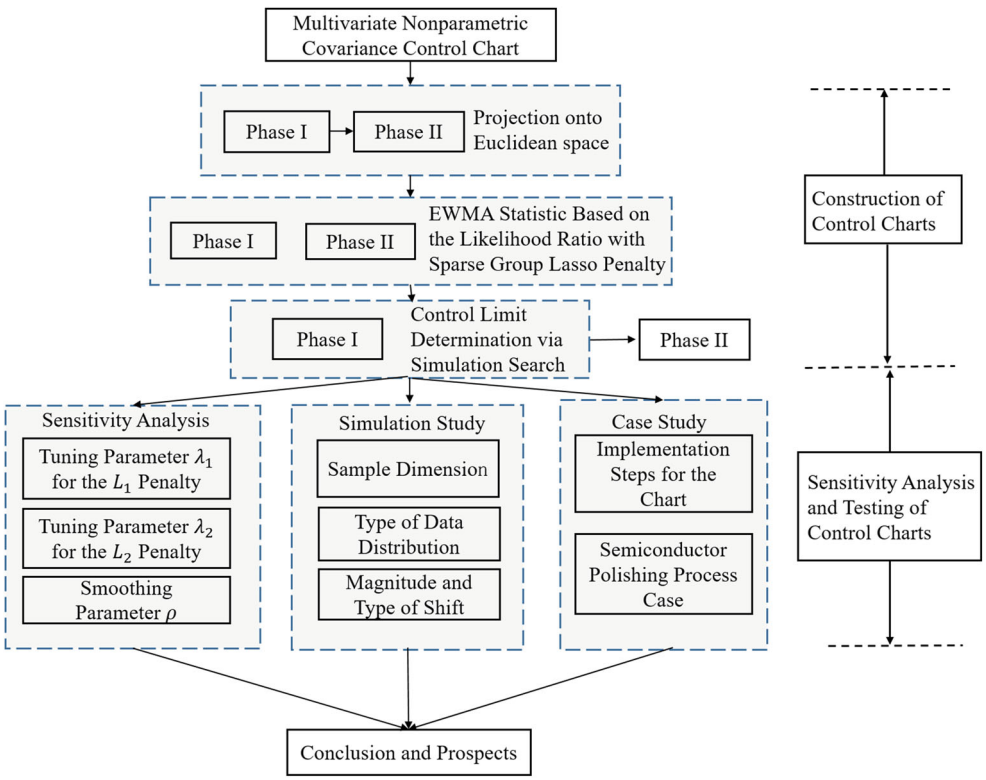

Figure 1. The structure of this paper.

2.1.1. The statistic in phase I

Let $Y_{n\times p}$ denote the sample obtained from a discrete sequence at time i $(i = 1, 2, \ldots, n)$, which contains a set of n points in p dimensions. Let $D_{n\times n}$ denote the square distance matrix between points in Y_i. $I_{n\times n}$ denotes the identity matrix, and $1_{n\times 1}$ is a vector with all elements equal to 1. We first transform $D_{n\times n}$ into the cross-product matrix $G_{n\times n}$. $G_{n\times n}$ can be obtained from the formula

$$G_{n\times n} = -\frac{1}{2} J_{n\times n} D_{n\times n} (J_{n\times n})^{\top}, \tag{5}$$

where $J_{n\times n} = I_{n\times n} - \frac{1}{n} 1_{n\times 1} 1_{n\times 1}^{\top}$. $G_{n\times n}$ preserves the distance relationships between each pair of points in $Y_{n\times p}$. We can obtain the coordinates of each point in Euclidean space based on the eigenvalue decomposition of $G_{n\times n}$:

$$G_{n\times n} = U_{n\times n} \Lambda_{n\times n} (U_{n\times n})^{\top}, \tag{6}$$

where $\Lambda_{n\times n}$ is the diagonal matrix formed by the eigenvalues of $G_{n\times n}$, and $U_{n\times n}$ is the matrix formed by the corresponding eigenvectors.

For further research, we need to determine the number of principal axes to be retained in $G_{n\times n}$, denoted as k. When selecting the value of k, it is necessary to include most of the information in the original data without including irrelevant random variations. We retain all axes of $G_{n\times n}$ with positive eigenvalues greater than 1. Therefore, the Euclidean principal

axes are

$$R_{n\times k} = U_{n\times n}\Lambda_{n\times k}^{1/2}, \tag{7}$$

where $\Lambda_{n\times k}$ is the eigenvalue matrix, and $U_{n\times n}$ is the eigenvector matrix. The Euclidean distance between each pair of points in $R_{n\times k}$ is approximately equal to the distance of points in $Y_{n\times p}$.

2.1.2. The statistic in phase II

In Phase II, we project new data onto the coordinate axes defined by $R_{n\times k}$. Let $Y_{n^*\times p}$ denote the new data observed in Phase II, where n^* is the number of observations. Calculate the distances between each element in $Y_{n^*\times p}$ and each element in $Y_{n\times p}$. Let $D^*_{n\times n^*}$ denote the distance matrix, and convert it to the cross-product matrix $G^*_{n\times n^*}$:

$$G^*_{n\times n^*} = -\frac{1}{2}J_{n\times n}(D^*_{n\times n^*} - D_{n\times n}e_{n\times 1}(1^*_{n^*\times 1})^\top). \tag{8}$$

Note that Equation (7) can be rewritten as

$$R_{n\times k} = (G_{n\times n})^\top U_{n\times n}\Lambda_{n\times k}^{-1/2}. \tag{9}$$

Replace $G_{n\times n}$ with $G^*_{n\times n^*}$. The coordinates of the new data in the projected space are

$$R^*_{n^*\times k} = (G^*_{n\times n^*})^\top U_{n\times n}\Lambda_{n\times k}^{-1/2}. \tag{10}$$

The coordinates $R^*_{n^*\times k}$ will be used in subsequent processes to calculate the EWMA-type statistics for the approximate Alt's likelihood ratio.

2.2. Covariance control chart based on sparse group Lasso penalty

The multivariate sample $Y_{n\times p}$ obtained from the discrete sequence at time i $(i = 1, 2, \ldots, n)$ is a set of n points in p dimensions. When the process is IC, we assume that $\mu = \mu_0$ and $\Sigma = \Sigma_0$. For the ith variable, its mean is μ_i, and its variance is σ_i^2 $(i = 1, 2, \ldots, p)$. The correlation coefficient between the ith and jth variables is ρ_{ij} $(i, j = 1, 2, \ldots, p)$. The mean vector and covariance matrix can be written as

$$\mu = (\mu_1, \mu_2, \mu_3, \ldots, \mu_p)^\top \quad \text{and} \quad \Sigma = \begin{pmatrix} \sigma_1^2 & \rho_{12}\sigma_1\sigma_2 & \cdots & \rho_{1p}\sigma_1\sigma_p \\ \rho_{21}\sigma_2\sigma_1 & \sigma_2^2 & \cdots & \rho_{2p}\sigma_2\sigma_p \\ \vdots & \vdots & \ddots & \vdots \\ \rho_{p1}\sigma_p\sigma_1 & \rho_{p2}\sigma_p\sigma_2 & \cdots & \sigma_p^2 \end{pmatrix}.$$

These parameters can be known or estimated from the Phase I data. When the process is OC, the covariance matrix changes from Σ_0 to Σ_{OC}. The proposed control chart is used to monitor the shift in the covariance matrix. First, a suitable penalty function is selected to estimate the sparse estimate of the projected covariance matrix. Then, a hypothesis is established, and an approximate Alt's likelihood ratio test statistic is calculated to test the hypothesis:

$$H_0 : \Sigma = \Sigma_0 \Longleftrightarrow H_1 : \Sigma = \Sigma_1.$$

Among these, $\Sigma_1 \neq \Sigma_0$, and Σ_1 differs from Σ_0 in three main OC scenarios:

(1) variance shift (changes in the variance σ_i of multiple variables);
(2) covariance shift (changes in the correlation coefficients ρ_{ij} between multiple pairs of variables);
(3) simultaneous variance and covariance shift (simultaneous changes in the variances σ_i and correlation coefficients ρ_{ij} of multiple variables).

These three different shift scenarios are simulated in Section 3.

Most multivariate covariance matrix control charts are based on the assumption of data normality, which means $Y_{n\times p}$ comes from a multivariate normal distribution. For example, Alt (1984) used the asymptotic distribution of the generalized likelihood ratio statistic to monitor the covariance of normally distributed data. Kim et al. (2019) improved Alt's method by using a parameter control chart based on the ridge-penalized likelihood ratio to monitor the covariance matrix. Nonparametric control charts include process monitoring using methods such as spatial rank, data depth, and nonparametric tests. There are also studies using other methods, such as Adegoke et al. (2022), which similarly improved Alt's method by using a Shewhart statistic based on the Lasso-penalized likelihood ratio to achieve nonparametric monitoring of covariance.

In this section, we first introduce the construction of the LGShewhart control chart (Adegoke et al., 2022) and the RGEWMA control chart (Kim et al., 2019), and then present our improved scheme, proposing a new control chart for monitoring covariance matrix shift, which is named the SGLGEWMA control chart ('SGL' means Sparse Group Lasso, and the second capital letter 'G' means GLR). The improvements primarily involve (1) obtaining a sparse full-rank estimate of the covariance matrix by solving an optimization problem based on the Sparse Group Lasso penalty, and (2) incorporating the influence of variance terms in the construction of monitoring statistics.

2.2.1. LGShewhart control chart and RGEWMA control chart

As mentioned above, Kim et al. (2019) improved Alt's method by monitoring the shift of the covariance matrix using a parameter control chart based on the likelihood ratio of the ridge penalty function. Similarly, building on Alt's research, Adegoke et al. (2022) utilized the Euclidean space projection mentioned in Subsection 2.1 and the Shewhart statistic based on the Lasso penalty likelihood ratio to achieve nonparametric monitoring of the covariance matrix. The following subsections briefly introduce the construction of the monitoring statistics for both control charts.

To obtain a full-rank estimate of the sample covariance matrix S, Kim et al. (2019) solved an optimization problem that differs from Equation (3):

$$\arg\max_{\Omega}\left\{\log|\Omega| - \operatorname{tr}(\Omega S) - \frac{\lambda}{2}\|\Omega\|_2^2\right\}. \tag{11}$$

The solution $\widehat{\Omega}$ to the above optimization problem is also a full-rank estimate of the precision matrix Ω, where the penalty term $\frac{\lambda}{2}\|\Omega\|_2^2 = \frac{\lambda}{2}\sum_{i=1}^{p}\sum_{j=1}^{p}(\omega_{ij})^2$, has an explicit solution $\widehat{\Omega} = [(\lambda I_p + \frac{1}{4}S^2)^{\frac{1}{2}} + \frac{1}{2}S]^{-1}$, and using the inverse of this result to replace S_i in the following equation yields the statistic w_i:

$$w_i = \operatorname{tr}(S_i) - \log|S_i| - p. \tag{12}$$

In the paper by Adegoke et al. (2022), the full-rank sparse estimate of the precision matrix $\boldsymbol{\Omega}$ is obtained by solving Equation (3), the optimization problem with the Lasso penalty term. This estimate is obtained using the Graphical Lasso algorithm, and the Shewhart statistic is constructed with Equation (12). Since Kim et al. (2019) employed a parametric method, we adapt it to the framework of this paper by constructing a nonparametric control chart using Euclidean space projection and the EWMA statistic based on the Ridge penalty likelihood ratio, enabling it to handle data from different distributions.

For the control limit, Adegoke et al. (2022) obtained them using a combination of the bootstrap algorithm and the quantile method. However, subsequent research found that the control limits obtained using this method were unstable. Therefore, both types of control charts and the proposed control chart use the simulation search method to get the control limit.

The two control charts mentioned above are named Lasso GLR Shewhart control chart (abbreviated as LGShewhart) (Adegoke et al., 2022) and RGEWMA control chart (Kim et al., 2019), respectively. In the following sections on statistical simulation and case studies, the performance of the proposed SGLGEWMA control chart will be compared with these two control charts.

2.2.2. The proposed SGLGEWMA control chart

Kim et al. (2019) and Adegoke et al. (2022) obtained full-rank estimates of the covariance matrix by solving optimization problems based on Ridge and Lasso penalties, respectively. Danaher et al. (2014) pointed out that when observations may come from multiple different distributions, Sparse Group Lasso-based penalties perform better. When estimating the sparsity matrix, Sparse Group Lasso not only encourages group sparsity but also allows for intra-group sparsity; moreover, in high-dimensional data, Lasso's sparsity selection may be influenced by noise, leading to unstable selection, especially for highly correlated variables.

In Phase I, the ith row of data r_i in $R_{n\times k}$ is the coordinate of the projected data at time point i, $S_i = r_i^\top r_i$, S_i is singular, and S_i is regularized by solving an optimization problem based on Sparse Group Lasso penalty:

$$\arg\max_{\boldsymbol{\Omega}_i}\{\log|\boldsymbol{\Omega}_i| - \operatorname{tr}(\boldsymbol{\Omega}_i S_i) - \lambda_1\|\boldsymbol{\Omega}_i\|_1 - \lambda_2\|\boldsymbol{\Omega}_i\|_2\}, \tag{13}$$

where ω_{ij} is the (i,j) entry of the precision matrix $\boldsymbol{\Omega}_i$, and λ_1, λ_2 are tuning parameters used to obtain different degrees of shrinkage for the estimate of $\boldsymbol{\Omega}_i$. $\lambda_1\|\boldsymbol{\Omega}_i\|_1 = \lambda_1\sum_{i=1}^k\sum_{j=1}^k|w_{ij}|$ and $\lambda_2\|\boldsymbol{\Omega}_i\|_2 = \lambda_2\sqrt{\sum_{i=1}^k\sum_{j=1}^k(\omega_{ij})^2}$ are the penalty terms, which ensure that the estimated precision matrix is invertible. This problem is solved using the ADMM algorithm described in Subsection 2.2.4.

When $\lambda_1, \lambda_2 \in (0,\infty)$, $\widehat{\boldsymbol{\Omega}}_i$ is a positive definite symmetric matrix; when $\lambda_1, \lambda_2 \to 0$, we have $\widehat{\boldsymbol{\Omega}}_i \to S_i^{-1}$; and when $\lambda_1, \lambda_2 \to \infty$, we have $\widehat{\boldsymbol{\Omega}}_i \to \mathbf{0}$. After selecting appropriate λ_1, λ_2, an effective estimate is obtained. If the process is IC, most elements remain unchanged; if the process is OC, the changes in the relationships between variables can be reflected in the estimate of $\boldsymbol{\Omega}$. We replace S_i in Equation (13) with the inverse of the estimated $\widehat{\boldsymbol{\Omega}}_i$, and propose a nonparametric EWMA control chart based on the Sparse Group Lasso penalty for effectively detecting shifts in the covariance matrix of individual observations in Phase II.

Throughout this paper, we focus on Phase II monitoring of individual observations, corresponding to a subgroup size of $m = 1$. In this setting, each incoming observation

is monitored sequentially without forming rational subgroups. This design is motivated by applications where data arrive one at a time (e.g., sensor streams or industrial process data), and immediate detection of shifts is required. Monitoring with $m > 1$ would introduce additional detection delay, which is undesirable in such scenarios.

In Phase II, $R^*_{n^*\times k}$ is the projection coordinate of the new sample, and the ith row data r_i^* of $R^*_{n^*\times k}$ is the coordinate of the data projection at time point i. The steps for obtaining the monitoring statistic w_i^* for the ith sample in Phase II are the same as in Phase I, where $i = 1, \ldots, n^*$, and H_i is the inverse of the Sparse Group Lasso penalty likelihood estimate of $S_i^* = r_i^{*\top} r_i^*$, obtained from the following equation:

$$\arg\max_{H_i} \left\{ \log|H_i| - \operatorname{tr}(H_i S_i^*) - \lambda_1 \|H_i\|_1 - \lambda_2 \|H_i\|_2 \right\}. \tag{14}$$

The monitoring statistics proposed by Adegoke et al. (2022) are Shewhart-type statistics, which cannot accumulate potential shift information. EWMA-type statistics do not have this defect, so we consider constructing EWMA-type statistics.

First, define the matrix $M_0 = I_k$, and then define an empty vector v. The EWMA-type statistic w_i based on the approximate Alt's likelihood ratio is given by the following steps.

(1) Calculate the projected sample covariance matrix S_i.
(2) Calculate the full-rank sparse estimate $\widehat{S_i}$ of S_i based on the ADMM algorithm.
(3) Let the maximum value on the diagonal of $\widehat{S_i}$ be denoted as v_i. Add v_i to the vector v and update the current mean $\bar{v}_i$ of v.
(4) Take $M_i = (1-\rho)M_{i-1} + \rho\widehat{S_i}$, and calculate $c_i = \operatorname{tr}(M_i) - \ln|M_i| - k$.
(5) Monitor the statistical quantity $w_i = c_i \times \bar{v}_i$.

For $i = 1, 2, \ldots, n$, $\rho \in (0, 1)$ is a smoothing parameter that determines the weight of the shift information for each observation, and $\widehat{S_i}$ is obtained by solving the optimization problem (13). The construction process of the above statistics in Step (4) draws inspiration from the ideas in the papers (Huwang et al., 2007; Yeh et al., 2005). M_i retains the shift information of each observation, so when the observations continue to shift, M_i accumulates the shift information of each covariance matrix.

During the simulation process, it was found that if only c_i from Step (4) is used as the monitoring statistic, it will be more sensitive to the shift of the covariance term and less effective in monitoring the shift of the variance term. v stores the maximum value of the variance term for each covariance matrix. Therefore, incorporating the influence of $\bar{v}_i$ in Step (5) results in the final monitoring statistic w_i being more effective in monitoring the shift of the covariance matrix. The theoretical derivation of the selection of monitoring statistics w_i and c_i and related experiments, with experimental details are presented in Subsection 2.2.3.

There are several methods to obtain the control limit h, including formula derivation, the bootstrap percentile method, the search method, etc. In this paper, the control limit is obtained through the Monte Carlo simulation search method.

When $w_i^* > h$, the control chart gives an OC message, where the control limit h is chosen to achieve the specified ARL_0. The flowchart of the EWMA control chart based on the Sparse Group Lasso penalty is shown in Figure 2.

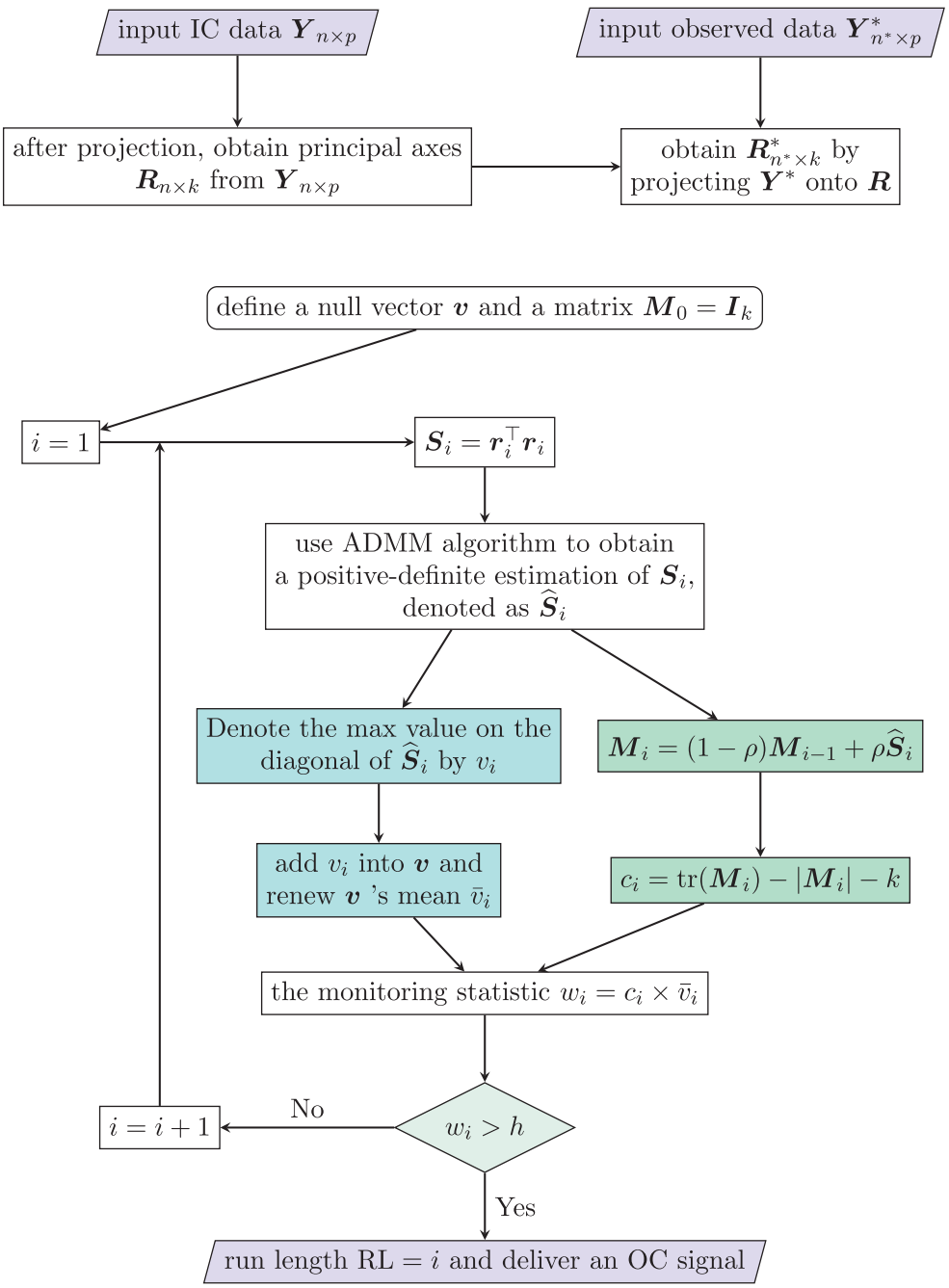

Figure 2. Flowchart of the EWMA control chart based on the Sparse Group Lasso.

2.2.3. A further discussion on the monitoring statistic

In Subsection 2.2.2, we present the construction process of the monitoring statistics w_i and c_i, followed by the theoretical basis and experiments for selecting w_i as the final monitoring statistic.

Table 1. ARL values of w_i and c_i under different scenarios, dimensions p, and shift magnitudes δ (values in parentheses correspond to Scenario III).

Scenario	p	Statistic	$\delta = 0$	0.1(0.2)	0.2(0.4)	0.3(0.6)	0.4(0.8)	0.5(1.0)	0.6(1.2)	0.7(1.4)	0.8(1.6)	0.9(1.8)
Scenario I	2	w_i	200.51	91.79	47.47	29.12	20.44	15.16	12.01	9.94	8.58	7.43
		c_i	199.34	108.54	68.18	47.20	33.82	25.38	20.73	17.15	14.35	12.38
	5	w_i	199.44	63.62	27.71	15.87	10.86	7.95	6.42	5.27	4.53	3.94
		c_i	199.28	89.03	47.25	28.91	19.87	15.01	11.66	9.57	8.03	7.06
	10	w_i	200.91	42.08	16.94	9.80	6.62	5.13	4.13	3.46	3.01	2.67
		c_i	200.86	70.30	32.41	18.61	12.47	9.27	7.39	6.20	5.33	4.62
	15	w_i	199.20	32.36	12.50	7.52	5.20	4.05	3.36	2.89	2.58	2.30
		c_i	200.41	58.82	24.46	13.97	9.56	7.21	5.92	5.00	4.36	3.90
Scenario II	2	w_i	199.75	189.22	164.16	130.25	100.16	76.59	61.58	49.47	42.17	34.02
		c_i	199.89	189.34	163.12	128.40	100.42	75.08	59.73	48.30	39.14	31.41
	5	w_i	199.80	173.47	118.30	76.75	51.79	37.33	28.37	23.26	19.62	16.66
		c_i	199.71	171.06	117.55	75.36	50.17	36.31	27.98	21.91	17.92	15.23
	10	w_i	200.86	189.55	156.47	112.67	83.90	63.75	49.53	38.28	31.00	26.40
		c_i	200.81	188.74	152.00	114.64	83.98	62.19	48.39	38.42	31.24	25.81
	15	w_i	199.49	193.06	168.37	139.32	112.96	85.88	67.69	53.46	44.75	37.98
		c_i	200.19	190.98	169.37	140.50	109.73	90.56	66.28	53.93	45.10	38.46
Scenario III	2	w_i	200.98	43.93	18.99	11.66	8.40	6.70	5.64	4.87	4.37	4.02
		c_i	198.86	64.03	29.32	17.86	12.96	10.34	8.55	7.39	6.45	5.79
	5	w_i	199.07	24.17	9.88	6.24	4.64	3.85	3.32	2.96	2.72	2.49
		c_i	200.17	39.14	16.31	10.06	7.43	5.95	5.02	4.39	3.91	3.63
	10	w_i	199.63	15.71	6.31	4.17	3.12	2.56	2.17	1.93	1.77	1.65
		c_i	198.56	29.88	11.53	7.12	5.24	4.14	3.53	3.10	2.74	2.50
	15	w_i	199.91	12.69	5.23	3.40	2.59	2.15	1.87	1.67	1.53	1.43
		c_i	200.02	23.64	9.55	5.85	4.36	3.56	3.05	2.69	2.39	2.20

Let $M_i = (1-\rho)M_{i-1} + \rho\widehat{S}_i$ be the smoothing covariance matrix, $c_i = \mathrm{tr}(M_i) - \ln|M_i| - k$, $v_i = \max_j \widehat{S}_{i,jj}$ and $\bar{v}_i$ be its running mean. Suppose there is a small shift on S_i and $\widehat{S}_i$ changes to $\widehat{S}_i^*$, denoted as $\Delta\widehat{S}_i = \widehat{S}_i^* - \widehat{S}_i$. Then $\Delta\widehat{S}_i$ is a small perturbation on $\widehat{S}_i$. Correspondingly, matrix $\Delta M_i = \rho\Delta\widehat{S}_i$ is a small perturbation on M_i. For ΔM_i, a matrix Taylor expansion yields

$$\delta c_i = \mathrm{tr}\left[(I - M_i^{-1})\Delta M_i\right] \text{ and } \delta w_i \approx \bar{v}_i\delta c_i + c_i\delta\bar{v}_i.$$

If the shift is variance-dominated at coordinate j (i.e., $\Delta\widehat{S}_i \approx \delta\sigma_j^2 E_{jj}$, where $\delta\sigma_j^2$ is a small change on σ_j^2, and E_{jj} is a matrix with the jth element on its diagonal equal to 1 and all other elements being 0.), then

$$\delta w_i \approx \left(\rho\bar{v}_i(1 - (M_i^{-1})_{jj}) + c_i\gamma\right)\delta\sigma_j^2, \tag{15}$$

where $\gamma = \frac{\delta\bar{v}_i}{\delta\sigma_j^2}$. δw_i is strictly positive for typical parameter settings and thus amplifies local variance changes. By contrast, for pure off-diagonal (covariance-only) perturbations $\delta\bar{v}_i \approx 0$ and the response reduces to $\delta w_i \approx \bar{v}_i\delta c_i$, which may be small or sign-indeterminate.

We also conduct additional simulation experiments to further investigate the detection properties of the proposed statistic w_i under finite-sample settings. Specifically, we considered multivariate normal data under three scenarios of covariance matrix shifts (Scenario I: variance-dominated shifts; Scenario II: covariance-dominated shifts; Scenario III: both variance and covariance shifts), with different dimensions ($p = 2, 5, 10, 15$) and varying shift magnitudes. A detailed description of the simulation steps can be found in Section 3. The results are summarized in Table 1.

In Scenario I and Scenario III, across almost all dimensions and shift magnitudes, w_i yields substantially smaller ARL_1 values compared to c_i, implying faster detection of variance deviations. This validates the theoretical intuition that incorporating the maximum diagonal element v_i strengthens sensitivity to variance-related changes, which are often critical in practice. In Scenario II, w_i and c_i exhibit nearly identical ARL performance. The inclusion of v_i does not deteriorate the monitoring power in these cases, thereby ensuring that w_i maintains efficiency comparable to c_i when variance shifts are absent.

Empirical results reveal a targeted trade-off: the statistic w_i provides significant improvements in Scenarios I and III involving variance shifts, at the cost of marginal performance loss in pure covariance shifts. This behaviour stems from the variance-focussed design of $\bar{v}_i$, establishing the method's primary utility for detecting mean-relevant variance changes.

2.2.4. ADMM algorithm

To obtain a full-rank sparse estimate of S_i, we need to solve the optimization problem (13), which is addressed using the ADMM algorithm. For a detailed introduction to the ADMM algorithm and its convergence properties, see Boyd et al. (2011).

To use the ADMM algorithm to solve problem (13), under the positive definite constraint $\mathbf{\Omega}$, the problem can be written as

$$\arg\max_{\mathbf{\Omega},Z}\{\log\det(\mathbf{\Omega}) - \mathrm{tr}(S\mathbf{\Omega}) - P(Z)\}. \tag{16}$$

The constraint is that $\mathbf{\Omega}$ is positive definite, and $Z = \mathbf{\Omega}$. The scaled augmented Lagrangian function for this problem is expressed as

$$L_\gamma(\mathbf{\Omega}, Z, U) = \log\det(\mathbf{\Omega}) - \mathrm{tr}(S\mathbf{\Omega}) - P(Z) - \frac{\gamma}{2}\|\mathbf{\Omega} - Z + U\|_F^2 + \frac{\gamma}{2}\|U\|_F^2. \tag{17}$$

Here, $\|\cdot\|_F$ denotes the Frobenius norm, U is the dual variable, and γ is the penalty parameter. The corresponding ADMM algorithm is obtained by iterating the following three simple steps. In the tth iteration, the steps are as follows.

(a) $\mathbf{\Omega}^{(t)} = \arg\max_{\mathbf{\Omega}}\{L_\gamma(\mathbf{\Omega}, Z^{(t-1)}, U^{(t-1)})\}$.
(b) $Z^{(t)} = \arg\max_{Z}\{L_\gamma(\mathbf{\Omega}^{(t-1)}, Z, U^{(t-1)})\}$.
(c) $U^{(t)} = U^{(t-1)} + (\mathbf{\Omega}^{(t)} - Z^{(t)})$.

Next, we will show in more detail the ADMM algorithm for solving the inverse covariance matrix estimation problem based on the Sparse Group Lasso penalty.

(1) Initialization: Set $\mathbf{\Omega} = I$, $U = \mathbf{0}$, and $Z = \mathbf{0}$.
(2) Penalty Parameter: Select a scalar $\gamma > 0$.
(3) Iterative Updates: For $t = 1, 2, 3, \ldots$, until convergence, update according to the following steps.
   (i) Update $\mathbf{\Omega}^{(t)}$ so that the following expression is maxmized:

$$\log\det(\mathbf{\Omega}) - \mathrm{tr}(S\mathbf{\Omega}) - \frac{\gamma}{2}\|\mathbf{\Omega} - Z^{(t-1)} + U^{(t-1)}\|_F^2. \tag{18}$$

   Let $VDV^\top$ be the eigenvalue decomposition of the matrix $S - \gamma Z^{(t-1)} + \gamma U^{(t-1)}$, where D is a diagonal matrix. The jth diagonal element of the resulting update is

given by

$$\frac{1}{2\gamma}\left\{-D_{jj}+(D_{jj}^2+4\gamma)^{1/2}\right\}.$$

(ii) Update $Z^{(t)}$ by maxmizing the following objective:

$$-\frac{\gamma}{2}\|Z-\Omega^{(t)}+U^{(t-1)}\|_F^2-P(Z). \tag{19}$$

(iii) Update the dual variable $U^{(t)}: U^{(t-1)}+\Omega^{(t)}-Z^{(t)}$.

The algorithm requires a penalty parameter γ to regulate the step size, as well as a convergence criterion. In this paper, we set $\gamma=1$ and define the convergence condition as follows:

$$\frac{\|\Omega^{(t)}-\Omega^{(t-1)}\|_F}{\|\Omega^{(t-1)}\|_F}<10^{-5}.$$

The convergence tolerance (10^{-5}) and penalty $\gamma=1$ follow the settings in the article (Danaher et al., 2014), which have been shown to provide stable estimates in practice. The details of maxmizing Equation (19) will depend on the form of the convex penalty function $P(\cdot)$. Solving the maxmization problem (19) can be rewritten as

$$\max_Z\left\{-\frac{\gamma}{2}\|\Omega^{(t)}-Z+U^{(t-1)}\|_F^2-P(Z)\right\}. \tag{20}$$

For Sparse Group Lasso penalties,

$$P(\Omega)=\lambda_1\sum_{i\neq j}|w_{ij}|+\lambda_2\left(\sum_{i\neq j}(w_{ij})^2\right)^{1/2}. \tag{21}$$

ADMM splits the optimization into simple subproblems – one maintaining positive definiteness of Ω, one applying sparsity penalties to Z, and one updating the dual variable U. Iterating these steps yields a sparse, full-rank precision matrix estimate. The flowchart of the ADMM algorithm with Sparse Group Lasso penalty is shown in Figure 3.

3. Statistical simulation

To test the monitoring performance of the proposed control chart, we need to conduct simulation experiments. In this section, we will test the proposed control chart by simulating data from different dimensions, distributions, and shift types, and compare the results with the control chart mentioned in Subsection 2.2.1 to demonstrate the excellent monitoring performance of the proposed control chart.

3.1. Simulated data

This section investigates the monitoring performance of the proposed EWMA control chart based on the Sparse Group Lasso penalty for covariance matrix shift. In the simulation process, three factors are considered.

(1) Sample dimensions: Take four cases, 2, 5, 10, and 15, respectively.

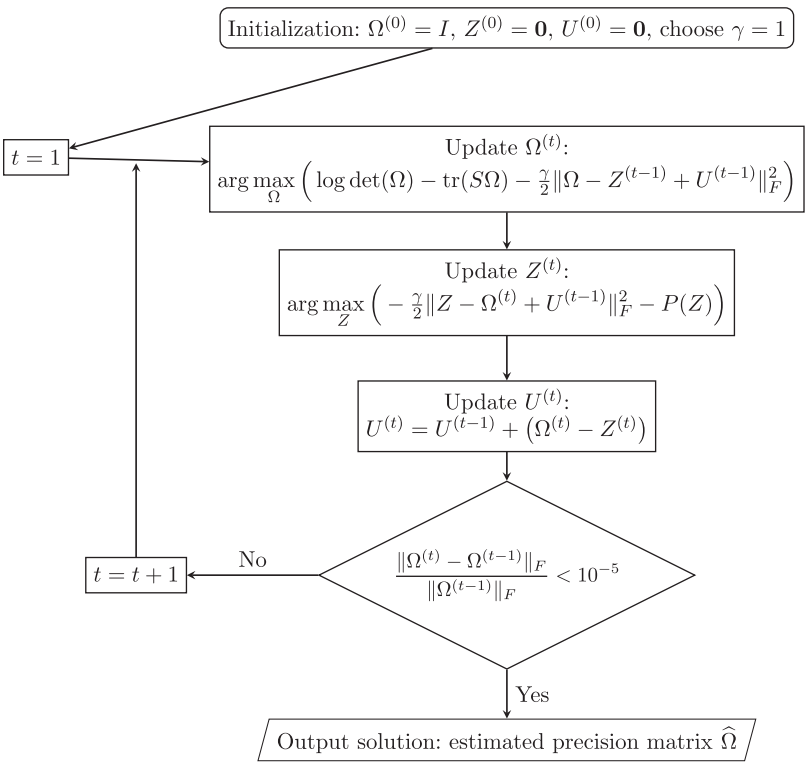

Figure 3. Flowchart of the ADMM algorithm with Sparse Group Lasso penalty.

(2) Distribution types of the monitored data, considering three types of distribution, including (i) discrete distribution: multivariate Poisson distribution (MPOIS); (ii) continuous distribution: multivariate normal distribution (MNORM) and multivariate gamma distribution (MGAMMA); (iii) mixed distribution: mixed distribution of multivariate Poisson distribution and multivariate normal distribution (MPOISNORM).

Among these, both MPOIS and MGAMMA data were simulated using a Gaussian Copula model to achieve a specific covariance matrix. The marginal parameters of MPOIS are $\mu \times 1_p$, where 1_p is a column vector of dimension p consisting of ones, $\mu = 2$; the mean vector of MNORM is the zero vector; the shape parameter and rate parameter of MGAMMA are set to $\alpha \times 1_p$ and $\beta \times 1_p$, respectively, with $\alpha = 4$ and $\beta = 1$; to simulate mixed distribution data with dimensions $p = 2, 5, 10, 15$, first simulate multivariate Poisson distribution data with dimensions $p_1 = 1, 2, 5, 8$ and marginal parameters $\mu \times 1_p$, then generate multivariate normal distribution data with dimensions $p_2 = p - p_1$ and zero mean vectors, and finally merge the data columns into mixed distribution data.

(3) Shift scenarios of the covariance matrix. Consider three types of shifts.

Scenario I: Variance shift (changes in the variance of multiple variables), such as in manufacturing, where a measurement item on a production line becomes more volatile due to wear and tear on the measuring instrument. In this scenario, the diagonal elements of the IC covariance matrix shift from 1 to $1 + \delta$, while the off-diagonal elements remain unchanged. Here, δ is the shift magnitude, with values ranging from 0.1 to 0.9 in increments of 0.1.

Scenario II: Covariance shift (changes in the correlation coefficient ρ_{ij} between multiple variables), such as in industrial process monitoring, where temperature and humidity were originally positively correlated, but due to a malfunction in the air conditioning system, the relationship between the two weakened or reversed. In this scenario, only the off-diagonal elements of the covariance matrix at positions $\{(i,j) \mid i,j = 1,2,3,(p-1)\}$ shift from 0 to δ, while the remaining off-diagonal elements and the variance (diagonal elements) are unchanged. The setting for δ is the same as in Scenario I.

Scenario III: Both variance and covariance shift (multiple variables simultaneously experience changes in variance σ_i and correlation coefficient ρ_{ij}, belonging to more complex system anomalies), such as overall production line anomalies, leading to increased volatility in all measurement items and disordered structural relationships between variables. In this simulation experiment, the diagonal elements of the covariance matrix shift from 1 to $1+\delta$, while the off-diagonal elements at positions $\{(i,j) \mid i,j = 1,2,3,(p-1)\}$ shift from 0 to δ, with the remaining off-diagonal elements unchanged. Here, δ ranges from 0.2 to 1.8 in increments of 0.2.

See Appendix to check the specific form of the OC covariance matrices in the above three scenarios.

3.2. Simulation steps

Based on the above control chart theoretical model, we conducted analysis and processing in Phase I and Phase II, respectively. In Phase I, we generated individual observations of size n and p dimensions from an IC multivariate normal distribution, with the covariance matrix set to the identity matrix. We then projected the simulated data onto k principal coordinates and used a search method to obtain the control limits of the control chart based on the projected data. Then, at each time i in Phase II, a random vector with a shifted covariance matrix but unchanged location parameters is generated from the aforementioned multivariate distribution.

Under the influence of the factors mentioned in Subsection 3.1, calculate the ARL values under IC and OC conditions.

When the process is IC, an OC signal is considered a false alarm, so we prefer a larger ARL_0. When the process is OC, a smaller ARL_1 means quicker detection of shift, so we prefer a smaller ARL_1. Generally, the quality of control charts is compared under the condition that ARL_0 is fixed, with a smaller ARL_1 indicating better monitoring performance. There are typically three calculation methods: the Markov chain method, the integral method, and the Monte Carlo random simulation method. This paper adopts the Monte Carlo random simulation method.

At the same time, we note that the proposed control chart has relatively high requirements for IC data. When the IC data generated in a single batch cannot adequately characterize the distribution characteristics of the data, the control chart's monitoring effectiveness will also be poor, the run length will fluctuate more significantly, and the control limits will be unstable. Therefore, when determining the control limits using the search method and calculating the ARL_1 after a shift, we generate K sets of IC data to obtain the average and thus an accurate ARL_0 and control limits. Additionally, for each set of IC data, we simulate and generate N sets of OC data with a size of n^* and a dimension of p, thereby obtaining the ARL_1 under that set of IC data.

Table 2. The ARL values across different dimensions and shift magnitudes under Scenario I.

		δ									
Distribution	p	0	0.1	0.2	0.3	0.4	0.5	0.6	0.7	0.8	0.9
MNORM	2	200.51	91.79	47.47	29.12	20.44	15.16	12.01	9.94	8.58	7.43
	5	199.44	63.62	27.71	15.87	10.86	7.95	6.42	5.27	4.53	3.94
	10	200.91	42.08	16.94	9.80	6.62	5.13	4.13	3.46	3.01	2.67
	15	199.20	32.36	12.50	7.52	5.20	4.05	3.36	2.89	2.58	2.30
MPOIS	2	199.26	105.98	60.52	38.98	27.88	21.78	17.59	14.64	12.51	11.10
	5	200.92	77.72	36.42	22.21	15.45	11.75	9.22	7.83	6.57	5.83
	10	199.78	54.02	23.13	13.55	9.38	7.16	5.76	4.88	4.30	3.71
	15	200.16	43.78	17.19	10.07	7.06	5.58	4.57	3.88	3.44	3.07
MGAMMA	2	200.15	102.94	59.10	37.90	26.75	20.55	16.97	13.98	12.08	10.55
	5	200.41	73.69	35.36	21.13	14.42	10.96	8.55	7.21	6.21	5.50
	10	200.29	54.03	22.41	12.85	9.02	6.87	5.54	4.65	3.99	3.58
	15	199.92	45.93	17.90	10.43	7.11	5.49	4.49	3.84	3.30	2.96
MPOISNORM	2	199.83	115.32	71.29	47.92	35.62	27.02	21.52	17.88	15.41	13.37
	5	200.82	92.25	47.64	28.90	19.84	14.70	11.47	9.11	7.79	6.82
	10	202.01	64.54	28.30	16.05	10.92	8.04	6.45	5.39	4.60	4.04
	15	200.02	50.21	20.15	11.38	7.90	6.00	4.78	4.14	3.61	3.23

3.3. Simulation results

In this section, we compare the monitoring performance of the SGLGEWMA control chart based on the Sparse Group Lasso penalty proposed with the RGEWMA control chart based on the Ridge penalty (Kim et al., 2019) and the LGShewhart control chart based on the Lasso penalty (Adegoke et al., 2022). Both are capable of nonparametric monitoring of the multivariate covariance of individual observations.

When comparing the performance of different control charts, we typically set ARL_0 to 200, which can be obtained by setting the control limit h. For the values of ARL, the average is calculated based on the squared Euclidean distance with $K = 100, n = 800, n^* = 600, N = 500$ simulation run lengths. Additionally, the penalty terms are set to adjust the compression parameters $\lambda_1 = 0.3, \lambda_2 = 0.025$, and the smoothing parameter $\rho = 0.2$. For LGShewhart, following Adegoke et al. (2022), the Lasso penalty parameter is set to 1.5; for RGEWMA, preliminary simulations indicated that a Ridge penalty parameter of 15 and a smoothing parameter of 0.2 yield the best monitoring performance.

The simulation results will be presented in four subsections below: Scenario I, Scenario II, Scenario III, and the influence of dimensions. These subsections essentially represent scenarios that may occur in reality and possess significant simulation value.

3.3.1. Scenario I

Table 2 presents the ARL values of the proposed control chart under Scenario I. It can be seen that the proposed control chart has the best detection performance for MNORM under Scenario I, and the detection performance improves with increasing dimension for all distributions; however, it has the worst monitoring performance for the mixed (MPOISNORM) distribution. Figure 4 shows the ARL comparison of the three control charts when $p = 15$ under Scenario I. It shows that the proposed chart outperforms the other two charts.

3.3.2. Scenario II

Table 3 presents the ARL values of the proposed control chart under Scenario II. It can be seen that the proposed chart has better detection performance for all types of distributions at

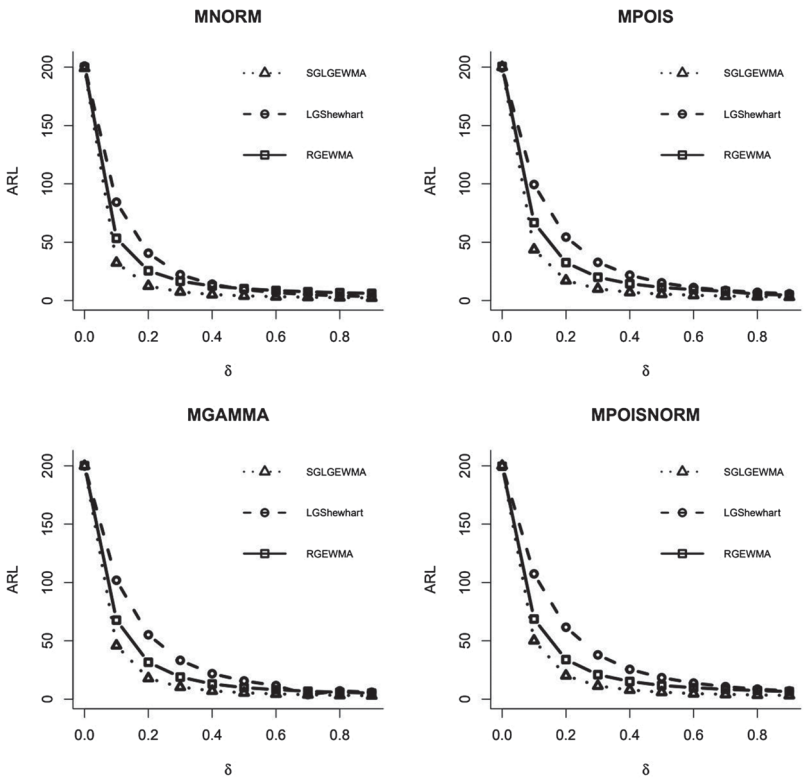

Figure 4. The ARL values as a function of δ when $p = 15$ (under Scenario I).

$p = 5$. Figure 5 shows the comparison of the ARL values for the three control charts at $p = 15$ under Scenario II. Compared to the other two charts, the proposed chart does not have an absolute advantage under Scenario II, but it does have an advantage when the distribution is multivariate normal or a mixture distribution with a large shift. However, under Scenario II, the proposed chart is not significantly different from the LGShewhart control chart, which has the best monitoring performance among the three.

3.3.3. Scenario III

Table 4 presents the ARL values of the proposed control chart under Scenario III. It can be seen that the detection performance of the control charts improves with increasing dimension, and they also exhibit better detection performance for data under the MNORM distribution. Figure 6 compares the ARL values of the three charts under Scenario III when $p = 15$. According to Figure 6, the proposed chart exhibits better detection performance than the others under Scenario III when $p = 15$.

3.3.4. The impact of dimensions

To study the monitoring performance of the proposed SGLGEWMA control chart in different dimensions, Tables 5 and 6 present comparisons of the ARL values in various dimensions between the proposed control chart and the RGEWMA control chart (Kim et al., 2019) (Overall, the RGEWMA control charts are more effective than the LGShewhart control charts in terms of monitoring) under Scenario I when the simulated data follow MPOIS and

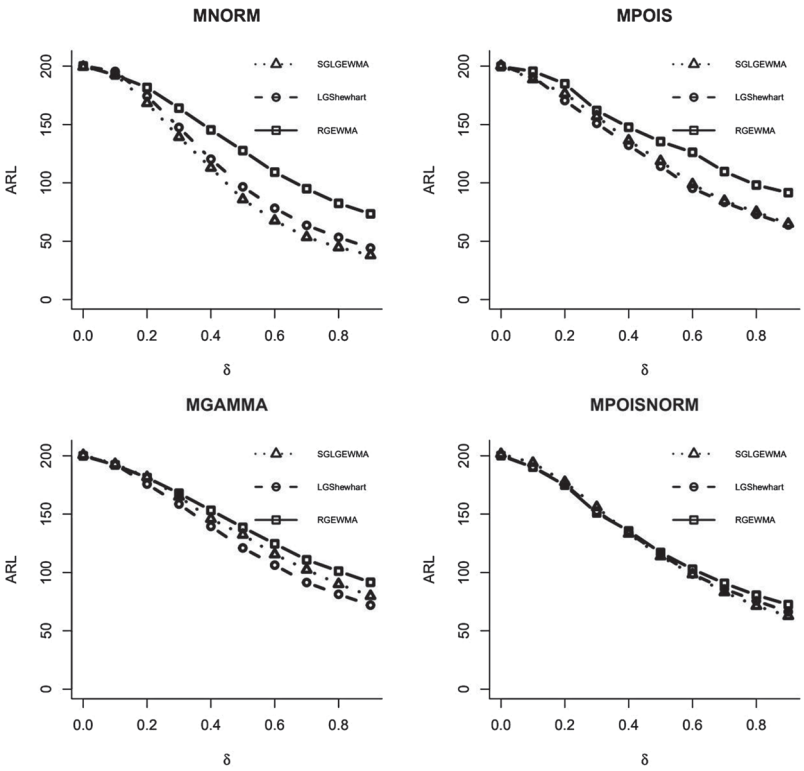

Figure 5. The ARL values as a function of δ when $p = 15$ (under Scenario II).

Table 3. The ARL values across different dimensions and shift magnitudes under Scenario II.

		δ									
Distribution	p	0	0.1	0.2	0.3	0.4	0.5	0.6	0.7	0.8	0.9
MNORM	2	199.75	189.22	164.16	130.25	100.16	76.59	61.58	49.47	42.17	34.02
	5	199.80	173.47	118.30	76.75	51.79	37.33	28.37	23.26	19.62	16.66
	10	200.86	189.55	156.47	112.67	83.90	63.75	49.53	38.28	31.00	26.40
	15	199.49	193.06	168.37	139.32	112.96	85.88	67.69	53.46	44.75	37.98
MPOIS	2	199.22	191.54	176.57	160.06	147.52	129.90	113.83	102.06	89.74	77.41
	5	200.21	178.08	143.55	113.58	91.20	71.67	59.05	51.51	41.82	37.31
	10	200.41	189.89	165.90	143.30	118.58	97.10	83.51	67.84	58.19	51.34
	15	200.26	188.71	176.53	157.03	136.27	118.64	98.77	84.52	75.14	64.97
MGAMMA	2	200.50	194.93	186.08	174.73	163.47	151.24	135.32	126.54	112.65	102.78
	5	199.23	181.61	161.27	134.21	110.45	93.86	80.78	71.44	65.20	54.09
	10	198.44	190.59	175.36	154.02	132.01	114.82	99.89	89.30	76.21	67.91
	15	200.59	192.88	181.76	165.01	145.87	132.37	115.51	102.37	90.05	79.89
MPOISNORM	2	200.10	195.09	189.87	184.58	175.50	165.58	151.95	147.35	133.67	129.99
	5	199.21	187.45	166.96	138.11	110.95	88.17	73.45	58.21	50.03	43.50
	10	200.37	186.92	166.38	142.15	116.20	95.75	79.36	65.66	56.28	47.29
	15	201.51	193.92	177.51	156.00	133.22	113.83	98.39	83.08	71.33	62.71

MNORM distributions. The results show that the proposed control chart exhibits superior monitoring performance across the given dimensions, with performance improving as the dimension increases (that is, the percentage reduction in ARL compared to the RGEWMA control chart increases with larger dimensions).

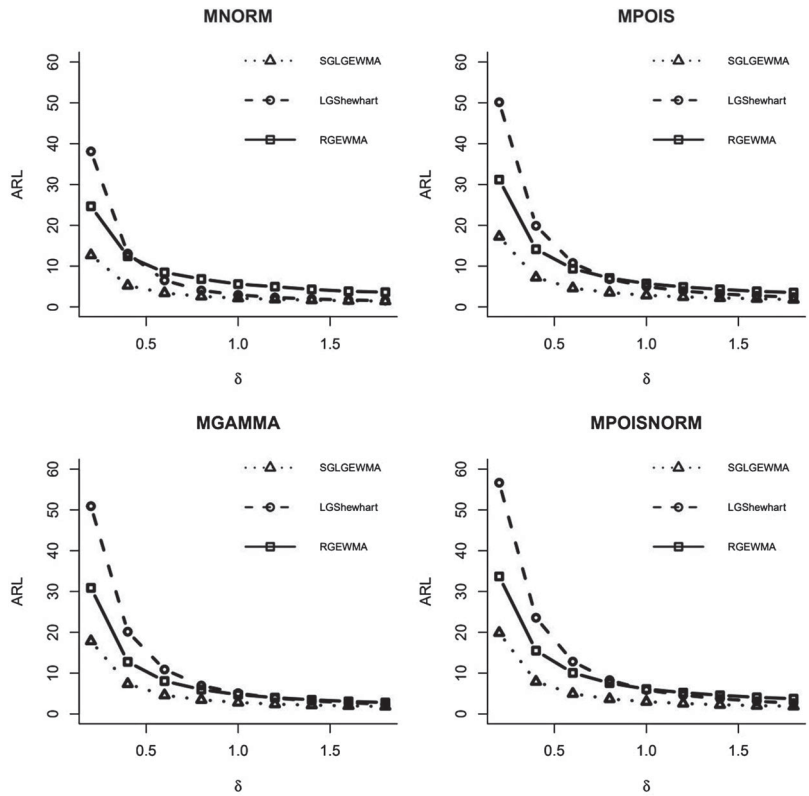

Figure 6. The ARL values as a function of δ when $p = 15$ (under Scenario III, values for $\delta = 0$ omitted).

3.4. Summary of simulation results

The tables above show the ARL_1 values of the proposed SGLGEWMA control chart as a function of dimension and shift magnitude under three different shift scenarios and four distributions: MNORM, MPOIS, MGAMMA, and MPOISNORM. The results in the tables indicate the following.

(1) The proposed SGLGEWMA control chart exhibits different performances in different distributions. Overall, when the data follows a MNORM distribution, the proposed chart detects a shift faster than other distributions. However, when the data follows a MPOISNORM distribution, if Scenario I or Scenario III occurs, the chart alerts more slowly than other distributions. For example, when $p = 5$ and detecting variance shift $\delta = \{0.1, 0.9\}$ (that is, Scenario I), the ARL_1 values are $\{63.62, 3.94\}$ under MNORM and $\{77.72, 5.83\}$ under MPOISNORM; under MGAMMA, it is $\{73.69, 5.50\}$ and under MPOISNORM it is $\{92.25, 6.82\}$.

(2) In Scenario I and Scenario III, the performance of the proposed control chart improves as the dimension p increases; in Scenario II, the best results are obtained when $p = 5$. This result is also expected, as in Scenario II that only 12 covariance elements shift when $p = 5, 10, 15$.

Table 4. The ARL values across different dimensions and shift magnitudes under Scenario III.

		δ									
Distribution	p	0	0.2	0.4	0.6	0.8	1	1.2	1.4	1.6	1.8
MNORM	2	200.98	43.93	18.99	11.66	8.40	6.70	5.64	4.87	4.37	4.02
	5	199.07	24.17	9.88	6.24	4.64	3.85	3.32	2.96	2.72	2.49
	10	199.63	15.71	6.31	4.17	3.12	2.56	2.17	1.93	1.77	1.65
	15	199.91	12.69	5.23	3.40	2.59	2.15	1.87	1.67	1.53	1.43
MPOIS	2	199.38	58.54	28.40	18.06	13.37	10.68	9.30	8.08	7.37	6.77
	5	199.20	34.22	15.08	9.73	7.29	6.00	5.14	4.65	4.20	3.89
	10	200.20	22.61	9.31	6.04	4.44	3.44	3.59	3.10	2.76	2.48
	15	200.62	17.23	7.22	4.59	3.52	2.84	2.47	2.20	2.01	1.80
MGAMMA	2	200.57	57.56	27.28	17.43	13.02	10.46	8.83	7.89	6.99	6.52
	5	200.09	33.49	14.53	9.28	7.06	5.83	5.01	4.41	3.95	3.67
	10	199.75	22.37	9.05	5.69	4.30	3.47	2.98	2.62	2.38	2.16
	15	201.70	17.85	7.37	4.59	3.47	2.82	2.41	2.16	1.99	1.84
MPOISNORM	2	199.66	70.24	34.21	21.13	14.97	11.34	9.59	8.07	7.08	6.33
	5	199.35	44.39	18.74	11.22	7.92	6.31	5.26	4.57	4.06	3.67
	10	200.55	27.24	10.87	6.77	4.86	3.90	3.30	2.86	2.58	2.33
	15	201.62	19.88	7.92	4.96	3.67	3.01	2.57	2.26	2.04	1.88

Table 5. The ARL values of RGEWMA control chart (1) and proposed control chart (2) for MPOIS data.

	$p=2$		$p=5$		$p=10$		$p=15$	
δ	(1)	(2)	(1)	(2)	(1)	(2)	(1)	(2)
0	200.24	200.51	200.80	199.44	200.39	200.91	200.61	199.20
0.1	133.94	**91.79**	102.38	**63.62**	86.36	**42.08**	66.80	**32.36**
0.2	95.65	**47.47**	59.12	**27.71**	43.67	**16.94**	32.55	**12.50**
0.3	69.74	**29.12**	39.34	**15.87**	26.41	**9.80**	20.01	**7.52**
0.4	53.90	**20.44**	27.52	**10.86**	17.74	**6.62**	14.42	**5.20**
0.5	43.29	**15.16**	20.97	**7.95**	12.88	**5.13**	11.26	**4.05**
0.6	35.31	**12.01**	16.90	**6.42**	10.12	**4.13**	9.37	**3.36**
0.7	29.44	**9.94**	14.02	**5.27**	8.25	**3.46**	7.96	**2.89**
0.8	25.13	**8.58**	12.03	**4.53**	7.02	**3.01**	5.44	**2.58**
0.9	21.55	**7.43**	10.43	**3.94**	6.03	**2.67**	4.71	**2.30**

Table 6. The ARL values of RGEWMA control chart (1) and proposed control chart (2) for MNORM data.

	$p=2$		$p=5$		$p=10$		$p=15$	
δ	(1)	(2)	(1)	(2)	(1)	(2)	(1)	(2)
0	199.99	199.26	199.49	200.92	199.83	199.78	199.89	200.16
0.1	111.81	**105.98**	85.28	**77.72**	64.92	**54.02**	53.35	**43.78**
0.2	70.62	**60.52**	45.22	**36.42**	30.92	**23.13**	25.53	**17.19**
0.3	47.36	**38.98**	28.95	**22.21**	20.35	**13.55**	16.63	**10.07**
0.4	34.60	**27.88**	20.99	**15.45**	15.11	**9.38**	12.48	**7.06**
0.5	26.81	**21.78**	16.41	**11.75**	11.76	**7.16**	10.19	**5.58**
0.6	22.16	**17.59**	13.34	**9.22**	10.06	**5.76**	8.62	**4.57**
0.7	18.65	**14.64**	11.49	**7.83**	8.75	**4.88**	7.58	**3.88**
0.8	16.10	**12.51**	9.90	**6.57**	7.58	**4.30**	6.75	**3.44**
0.9	13.98	**11.10**	8.86	**5.83**	6.70	**3.71**	6.16	**3.07**

(3) The proposed control chart is the most effective in detecting Scenario III, followed by Scenario I. However, it is less effective in detecting Scenario II than the other two scenarios.

(4) We also compare the performance of the proposed SGLGEWMA control chart with the LGShewhart control chart and the RGEWMA control chart. Under the specified

$p = 15$, the results indicate that for the distributions under discussion, the proposed SGLGEWMA control chart outperforms the other two control charts in terms of performance under both Scenario I and Scenario III, and it also provides better detection performance for both large and small shifts. However, under Scenario II, the LGShewhart control chart performs better under the MPOIS and MGAMMA distributions, while the SGLGEWMA control chart demonstrates good monitoring performance under the MNORM distribution and large shifts in the MPOISNORM distribution. Overall, the proposed SGLGEWMA control chart exhibits superior monitoring performance.

(5) The results of the dimensionality analysis show that the proposed control chart has better monitoring effects in several given dimensions, and the larger the dimension, the better the effect.

4. Sensitivity analysis

The design of control charts involves the selection of parameters, which depend on the shift scenario, shift magnitude, and data distribution. In this section, we will study the changes in control chart monitoring performance caused by the penalty term tuning parameters λ_1, λ_2 and the smoothing parameter ρ. When studying the penalty term tuning parameters, we analyze the monitoring effects under three different shift scenarios, with the distribution set as a multivariate normal distribution and dimension $p = 10$. When studying the sensitivity of the smoothing parameter, we conduct separate studies on multivariate Poisson distribution and multivariate normal distribution data, while considering Scenario I shift and dimension $p = 10$. The L_1 penalty term tuning parameter λ_1 will consider five cases: $\lambda_1 = 0.2, 0.3, 0.4, 0.5, 0.6$. The L_2 penalty term tuning parameter λ_2 will be considered for five cases: $\lambda_2 = 0.025, 0.05, 0.75, 0.1, 0.2$. The smoothing parameter ρ will be considered for five cases: $\rho = 0.1, 0.2, 0.3, 0.4, 0.5$. Since the target $\mathrm{ARL}_0 = 200$, the ARL_0 values have been excluded from the figures in this section.

4.1. Tuning parameters

An important factor to the usage of Equation (13) or (14) is the selection of tuning parameters. λ_1, λ_2 are the tuning parameters of the penalty term, used to achieve different degrees of shrinkage in the estimation of $\mathbf{\Omega}_i$. The penalty term ensures that the estimated precision matrix is invertible and sparse. Sparse Group Lasso not only encourages group sparsity but also allows for intra-group sparsity when estimating the sparsity matrix. In high-dimensional data, the sparsity selection of Lasso may be influenced by noise, leading to unstable selection, especially for highly correlated variables. As proposed in Subsection 2.2.2, selecting appropriate λ_1 and λ_2 will yield effective estimates. If the process is IC, most elements remain unchanged. If the process is OC, the relationships between variables can be reflected in the estimates of $\mathbf{\Omega}$.

Tuning parameters are often set in a pragmatic manner to balance sparsity and interpretability (S. Li et al., 2013; Meinshausen & Bühlmann, 2010). As emphasized in prior work, approaches such as cross-validation(CV), BIC, or AIC may lead to overly dense works that are less useful for exploratory or hypothesis-generating purposes. For this reason, an application-driven choice is often more appropriate to ensure models remaining both interpretable and plausible.

The k-fold CV score for a generic regularized estimate $\widehat{\Omega}_{\lambda_1,\lambda_2}$ based on fixed λ_1, λ_2 is given as

$$\mathrm{CV}(\lambda_1, \lambda_2) = -\sum_{k=1}^{K} n_k \{\mathrm{tr}(S^{(k)}\widehat{\Omega}^{(-k)}_{\lambda_1,\lambda_2}) + \log|\widehat{S}^{(-k)}_{\lambda_1,\lambda_2}|\} \tag{22}$$

where n_k is the size of subset k, for $k = 1, \ldots, K$ disjoint subsets, $S^{(k)}$ is the sample covariance matrix based on subset k, $\widehat{S}^{(-k)}_{\lambda_1,\lambda_2}$ and $\widehat{\Omega}^{(-k)}_{\lambda_1,\lambda_2}$ are the estimated covariance matrix and precision matrix excluding subset k, respectively. The proper λ_1, λ_2 that maxmize the $\mathrm{CV}(\lambda_1, \lambda_2)$ score can be selected via a grid search.

However, as in our setting, the proposed chart monitors individual observations ($m = 1$ in Phase II), meaning that each new observation is sequentially incorporated into the monitoring statistic, rather than aggregated in rational subgroups. The use of such CV-based procedures becomes less practical. This is consistent with prior work (Adegoke et al., 2022). Computing the performance of the proposed chart over a range of values for λ_1 and λ_2 may be computationally onerous. We can search densely over λ_1 when holding λ_2 at a fixed low value. Then, holding λ_1 at the selected value, we conduct a quick search over λ_2. Following Danaher et al. (2014), we set $\lambda_1 \in [0.2, 0.6], \lambda_2 \in [0.025, 0.2]$, which ensure comparability and computational feasibility.

4.1.1. L_1 penalty term tuning parameter λ_1

In this paper, we discuss the changes in sensitivity caused by different shift scenarios and different shift magnitudes δ, as well as five cases of $\lambda_1 = 0.2, 0.3, 0.4, 0.5, 0.6$, when the L_2 penalty term tuning parameter is set to 0.025, the smoothing parameter $\rho = 0.2$, and the distribution is a multivariate normal distribution. When λ_1 is too large or too small, the resulting $\widehat{\Omega}_i$ becomes irreversible within the accuracy range. As shown in Figure 7, under Scenario I and Scenario III, the differences in ARL_1 under various λ_1 values are not very significant, while the differences are relatively larger under Scenario II. Overall, when $\lambda_1 = 0.3$, all types of shifts exhibit good monitoring performance.

4.1.2. L_2 penalty term tuning parameter λ_2

When the L_1 penalty term tuning parameter is set to 0.3, the smoothing parameter $\rho = 0.2$, and the distribution is a multivariate normal distribution, the changes in sensitivity caused by different shift scenarios and different shift degrees δ, $\lambda_2 = 0.025, 0.05, 0.75, 0.1, 0.2$ are examined. As shown in Figure 8, as λ_2 increases, the ARL_1 also increases, except when $\lambda_2 = 0.05$ under Scenario II, which yields the best monitoring performance. Overall, $\lambda_2 = 0.025$ provides good monitoring performance.

4.2. Smoothing parameter ρ

The EWMA control chart utilizes historical information during the monitoring process and is highly effective in monitoring small and medium-sized shifts. Since its introduction, the EWMA control chart has been extensively studied by researchers worldwide. The smoothing parameter ρ, a crucial parameter in EWMA control charts, has also received significant attention. Lucas and Saccucci (1990) indicated that when ρ takes a smaller value, the EWMA control chart performs better in detecting small shifts; when ρ takes a larger value, the EWMA control chart performs better in detecting larger shifts. In prior work

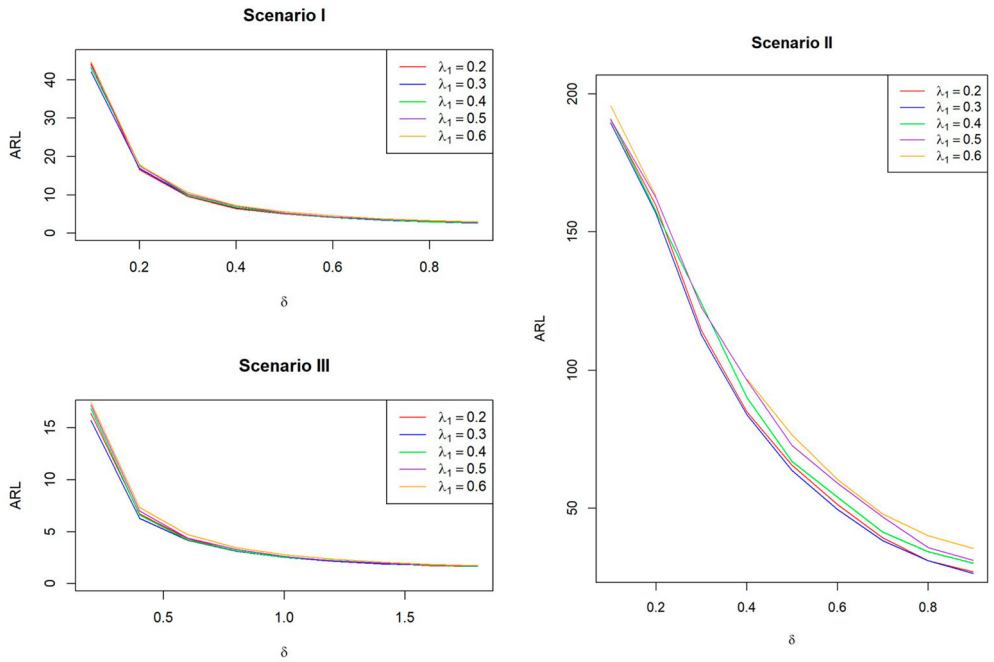

Figure 7. The effect of parameter λ_1 on monitoring effectiveness.

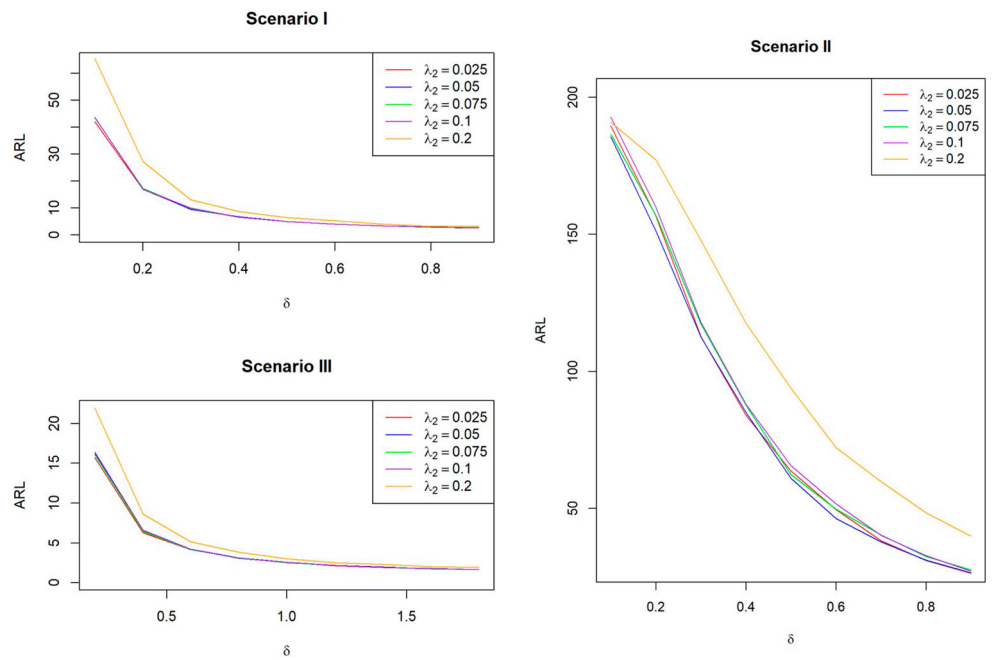

Figure 8. The effect of parameter λ_2 on monitoring effectiveness.

(Hawkins & Maboudou-Tchao, 2008; Lowry et al., 1992), ρ values between 0.1 and 0.3 are recommended for practical applications.

This paper examines changes in sensitivity under five distinct scenarios. The tuning parameters are fixed at $\lambda_1 = 0.3$ and $\lambda_2 = 0.025$, and the shift type is specified as Scenario

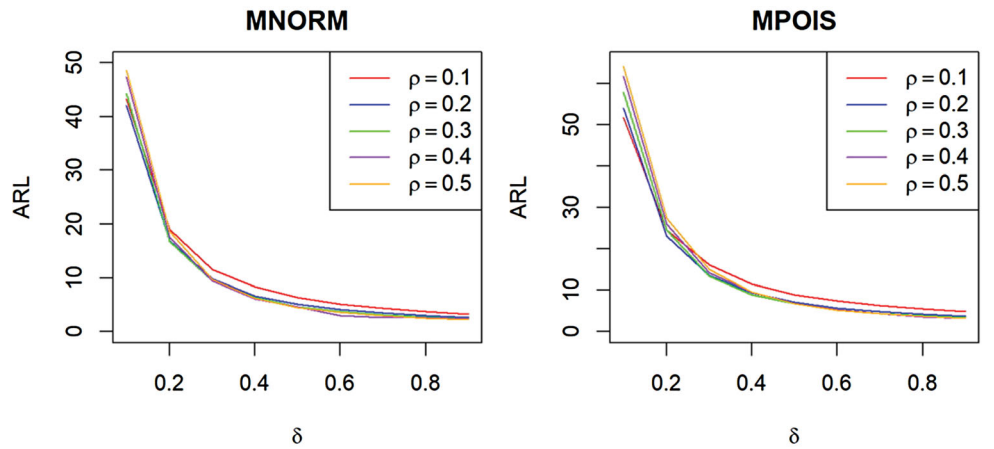

Figure 9. The effect of parameter ρ on monitoring effectiveness.

Table 7. The effect of parameter ρ on ARL_1 values under Scenario I.

		δ									
Distribution	ρ	0	0.1	0.2	0.3	0.4	0.5	0.6	0.7	0.8	0.9
MNORM	0.1	200.63	43.31	18.96	11.52	8.35	6.38	5.11	4.39	3.78	3.30
	0.2	200.91	**42.08**	16.94	9.80	6.62	5.13	4.13	3.46	3.01	2.67
	0.3	200.59	44.33	**16.84**	**9.50**	6.38	4.64	3.71	3.16	2.73	2.46
	0.4	200.30	47.38	17.48	**9.50**	**6.16**	4.65	**3.06**	**2.60**	2.60	2.37
	0.5	200.06	48.58	18.66	9.73	6.26	**4.49**	3.60	3.00	**2.53**	**2.33**
MPOIS	0.1	200.91	**51.71**	24.49	16.12	11.54	8.90	7.52	6.37	5.49	4.83
	0.2	199.78	54.02	**23.13**	13.55	9.38	7.16	5.76	4.88	4.30	3.71
	0.3	200.88	57.92	24.62	**13.51**	**8.94**	6.87	5.37	4.45	3.86	3.43
	0.4	200.04	61.70	26.00	14.32	9.61	**6.77**	5.43	4.44	**3.68**	**3.26**
	0.5	199.43	64.24	27.46	15.02	9.64	6.80	**5.22**	**4.41**	3.72	3.31

I and $p = 10$. The scenarios comprise the multivariate Poisson distribution and the multivariate normal distribution. For each distribution type, sensitivity is evaluated across varying shift magnitudes δ and smoothing parameters ρ (specifically, $\rho = 0.1, 0.2, 0.3, 0.4, 0.5$). This range covers the recommended values and additionally allows us to evaluate robustness in slightly larger ρ settings.

As shown in Table 7 and Figure 9, for different distributions, as ρ decreases, the detection performance for smaller shifts improves, while the detection performance for larger shifts weakens, but the differences are not significant. This conclusion is consistent with that of Lucas and Saccucci (1990). When $\rho = 0.2$, the monitoring performance is excellent for both larger and smaller shifts. Therefore, in the control chart simulation process in Section 3, we select $\rho = 0.2$ as the parameter.

5. Computational cost

An additional practical concern in the design of nonparametric control charts is their computational feasibility, especially in high-dimensional or large-sample settings. The proposed SGLGEWMA chart involves repeated eigen-decompositions and ADMM iterations to obtain

Table 8. Average runtime (seconds) per replication under $ARL_0 = 200$, with $\lambda_1 = 0.3, \lambda_2 = 0.025, \rho = 0.2$.

Case 1: $n = 800, n^* = 600$							
p	2	5	10	15	25	35	50
t	0.134	0.306	0.888	1.675	4.517	7.913	15.397
Case 2: $p = 10, n^* = 600$							
n	300	400	500	600	700	800	900
t	0.843	0.853	0.861	0.870	0.881	0.888	0.906
Case 3: $p = 10, n = 800$							
n^*	300	400	500	600	700	800	900
t	0.869	0.871	0.882	0.888	0.891	0.899	0.903

sparse full-rank covariance estimates, which could raise concerns about scalability. We conducted additional experiments under the setting $\lambda_1 = 0.3, \lambda_2 = 0.025, \rho = 0.2$ and the target $ARL_0 = 200$. Table 8 reports the average runtime (in seconds) per replication. The results show that (i) runtime increases moderately with the data dimension p (e.g., from 0.13 s at $p = 2$ to about 15.4 s at $p = 50$), (ii) the effect of enlarging Phase I sample size n or Phase II sample size n^* is relatively minor (remaining below 1s per replication), and (iii) the computational cost remains well within practical feasibility.

The results show that the majority of computational time is spent on solving the ADMM subproblems. As reported in Danaher et al. (2014), the worst-case computational complexity is $\mathcal{O}(p^3)$, primarily due to repeated eigenvalue decompositions. To address scalability, one promising direction is block-wise ADMM, where the estimated inverse covariance matrices $\widehat{\Omega}$ are block-diagonal with R blocks, each of size p_r ($\sum_{r=1}^{R} p_r = p$), reducing the complexity to $\sum_{r=1}^{R} \mathcal{O}(p_r^3)$.

Despite a non-negligible computational cost, particularly in high-dimensional settings, our empirical evaluation demonstrates that the method remains practical for moderate values of p. For real-time SPM applications, we recommend employing efficiency-enhancing strategies such as block-wise ADMM or parallel implementations to further mitigate the computational overhead.

6. Case study

6.1. Demonstration of the proposed monitoring scheme

In this subsection, we generate simulated data for Phase I observations under IC conditions ($n = 500$) and Phase II observations under OC conditions $n^* = 30$ to demonstrate the proposed monitoring scheme. IC observations are drawn from a multivariate Poisson distribution with $p = 10$ (simulated using a Gaussian copula model), with marginal parameters $\mu \times 1_p$ ($\mu = 2$). The OC observations come from a multivariate Poisson distribution with the same marginal parameters under Scenario I, and the variance elements shifting from 1 to $1 + \delta$, where δ is set to 0.6.

As described in the preceding sections, the monitoring is divided into two phases: Phase I and Phase II. In Phase I, we project the observed n p-dimensional IC data onto a Euclidean space of smaller or equal dimension. Then, using the projected coordinates, we obtain the control limit via a simulated search method. In Phase II, we project the n^*p-dimensional OC data onto the coordinate axes determined in Phase I. We calculate the EWMA statistic under

Table 9. Demonstration of the proposed monitoring scheme based on simulated data.

		Y				R		
Phase	i	y_1	y_2	y_{10}	r_1	r_2	r_{10}	w_i
Phase I	1	1	3	2	1.700	0.973	1.094	2.574
	2	5	4	1	0.201	−1.314	−2.780	16.262
	3	1	1	3	0.662	1.286	1.328	16.432
	4	7	4	2	1.870	−1.805	−3.020	44.714
	5	2	1	3	0.334	−0.610	−0.789	42.025
	…	…	…	…	…	…	…	…
	498	1	3	2	−1.612	−0.730	−0.461	90.088
	499	3	2	1	−0.611	−1.260	−0.439	74.594
	500	3	2	1	−0.735	−0.690	−0.617	70.726
Phase II	1	1	0	2	−1.448	0.264	0.480	6.945
	2	0	1	2	1.380	0.383	0.831	36.409
	3	2	1	1	−0.823	−0.314	0.199	25.035
	4	4	4	7	−1.217	2.177	−0.517	67.054
	5	2	8	7	1.133	3.122	0.187	93.842
	6	2	4	1	−0.971	−0.095	−1.252	98.340
	7	0	2	0	0.406	2.218	1.823	113.998
	8	2	2	3	−0.016	−0.698	0.394	87.180
	9	3	1	3	−0.122	−0.028	3.699	**151.785***
	10	6	1	4	2.444	−1.010	−2.036	**154.346***
	11	4	1	0	−0.629	−2.454	−2.670	**170.168***
	12	0	4	0	−1.320	0.382	0.681	**179.798***
	13	5	0	1	0.744	−3.958	−0.253	**175.785***
	14	4	0	1	0.513	−1.868	−1.895	**300.408***
	15	0	4	2	0.897	0.955	0.841	**236.955***
	…	…	…	…	…	…	…	…
	29	0	4	2	−1.011	3.301	2.601	**174.982***
	30	2	3	0	1.063	−0.456	0.500	**159.935***

the Sparse Group Lasso penalty for the Phase II projected sample and compare it with the control limit h determined in Phase I. The steps are as follows.

(1) Calculating distances and centralization matrix: Calculate the Euclidean distance squared matrix $D_{500\times500}$ for Phase I data, and construct the Gower centralization matrix G based on D;
(2) Principal coordinate analysis: Perform eigenvalue decomposition on G, extract the eigenvectors corresponding to the eigenvalues that meet the conditions, and obtain the principal coordinate matrix $R_{500\times10}$;
(3) Determining the control limit: Construct the EWMA statistic based on $R_{500\times10}$, and obtain the control limit h ($h = 137.15$) through Monte Carlo simulation;
(4) Calculating the Phase II projection: For the Phase II data Y^*, calculate its distance from the Phase I samples $D^*_{500\times30}$, and construct the Gower normalization matrix G^*, projecting G^* onto the main coordinate axes determined in Step (2) to obtain $R^*_{30\times10}$;
(5) Calculating monitoring statistics and triggering an alarm: Calculate the EWMA statistic w_i^* using R^*. If $w_i^* > h$, it is considered an outlier, and an alarm is triggered.

Table 9 shows the data during the monitoring process. Due to space limitations in the paper, the data for $y_3 \sim y_9$ and $r_3 \sim r_9$ have been omitted. $*$ indicates an OC signal, where $w_i > h$ (137.15).

The monitoring process of the results in Step (5) is shown in Figure 10, where the first 500 samples are IC and the last 30 data points are OC (separated by a red dashed line). The

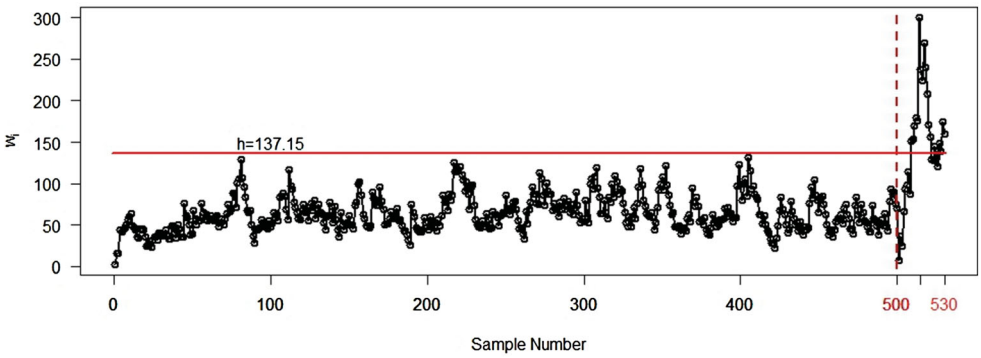

Figure 10. The monitoring process during Phase I and Phase II based on simulated data.

control limit $h = 137.15$ for this situation was obtained in the simulation in Section 3. As shown in Table 9 and Figure 10, in Phase I, all monitoring statistics are below the control limit h, and no alarms occur; in Phase II, at the 9th observation, the control chart triggers an alarm, and there are a total of 18 monitoring statistic values above the control limit. This result is not significantly different from the simulation results in Table 2.

6.2. *Illustration : grinding processes in wafer semiconductor manufacturing*

In this subsection, we will use grinding process data from wafer semiconductor manufacturing to demonstrate the proposed control chart. During the grinding process, saw marks are removed from the wafer, and variations in thickness are also reduced. J. Li et al. (2013) conducted preliminary research on this issue, and subsequently (Adegoke et al., 2022; Kim et al., 2019) also used this data set to evaluate the performance of the charts they proposed.

The wafer grinding process is primarily characterized by five variables: total thickness variation (Y_1), total indicator reading (Y_2), on-site total indicator reading (Y_3), bow (Y_4), and warp (Y_5). Any deviation of these variables beyond their specified tolerance limits can adversely affect the wafer grinding process, ultimately reducing the production yield of semiconductors. Therefore, these variables must be closely monitored and kept IC during production. The IC variance matrix (Σ_{IC}) and OC variance matrix (Σ_{OC}) for the grinding process are estimated by J. Li et al. (2013). Specifically, Σ_{IC} and Σ_{OC} are defined as follows:

$$\Sigma_{\text{IC}} = \begin{pmatrix} 1.30 & 0.46 & 0.51 & 0 & 0 \\ 0.46 & 1.30 & 0.53 & 0 & 0 \\ 0.51 & 0.53 & 1.30 & 0 & 0 \\ 0 & 0 & 0 & 1.30 & 0 \\ 0 & 0 & 0 & 0 & 1.30 \end{pmatrix},$$

$$\Sigma_{\text{OC}} = \begin{pmatrix} 1.30 & 0.62 & 0.63 & 0 & 0 \\ 0.62 & 1.30 & 0.68 & 0 & 0 \\ 0.63 & 0.68 & 1.30 & 0 & 0 \\ 0 & 0 & 0 & 1.30 & -0.55 \\ 0 & 0 & 0 & -0.55 & 1.30 \end{pmatrix}.$$

We assume that the covariance matrix of the wafer grinding process changes from Σ_{IC} to Σ_{OC}, and only the covariance matrix is available, while the complete dataset is unavailable. To construct the control chart for Phase II, we generate $n^* = 600$ observations from a multivariate normal distribution with a mean vector of zero and the OC covariance matrix Σ_{OC}.

Following the steps outlined in Section 2 and using the same parameter settings as in Section 3, we obtain the control limits for the LGShewhart, RGEWMA, and SGLGEWMA control charts as 21.1, 15.1, and 21.35, respectively. When $ARL_0 = 200$, the ARL_1 values of the three control charts during OC periods are 131.47, 143.61 and 97.48, respectively, clearly demonstrating that the proposed control chart provides better monitoring performance.

To better illustrate the comparison between the control charts, we have selected the OC data from one simulation for display. In Figure 11, the red dots indicate the first detection of an alarm signal. It can be seen that for this set of OC data, the proposed SGLGEWMA control chart issued an OC signal at the 29th observation, while the LGShewhart control chart and RGEWMA control chart issued OC signals at the 152nd and the 155th observation, respectively. Additionally, the LGSheWhart control chart issued 6 alarms, the RGEWMA control chart issued 8 alarms, and the SGLGEWMA control chart issued 9 alarms. In summary, the proposed control chart can effectively reduce losses caused by the delayed issuance of OC signals.

7. Summary and future prospects

7.1. Summary

With the development of industrial and big data technologies, new techniques are constantly being applied to quality control in industrial settings. During production processes, a large amount of data is collected, which is often highly complex. Therefore, how to effectively monitor the quality of such complex data has become a hot topic in current research. In most cases, these data exhibit a wide variety of data types, high data dimensions, and unclear data correlations. Under such circumstances, the assumption of multivariate normality is often invalid, necessitating the establishment of multivariate nonparametric control charts.

Regardless of whether the data variables are continuous, discrete, or a mixture of continuous and discrete, the proposed control charts can effectively monitor the covariance matrix of these complex data variables and alert them promptly to fluctuations. Our method first projects the IC data collected in Phase I into a Euclidean space of the same or lower dimension. Using the projected coordinate data, we calculate the approximate Alt's likelihood ratio EWMA statistic based on the Sparse Group Lasso penalty. Next, control limits that satisfy a specific ARL_0 are obtained through Monte Carlo simulation searches. Individual observations from Phase II are then projected onto the principal coordinates determined in Phase I, and the Alt's likelihood ratio EWMA statistic based on the Sparse Group Lasso penalty is similarly calculated. This statistic is compared with the control limit, and a shift is detected if it exceeds the control limit.

The results of the simulation statistics indicate that the proposed SGLGEWMA control chart can effectively monitor covariance matrix shift and outperforms the RGEWMA control chart based on Ridge penalty (Kim et al., 2019) and the LGShewhart control chart based on Lasso penalty (Adegoke et al., 2022) in monitoring Scenario I and Scenario III shifts. Additionally, the study found that, compared to the control chart based on the Ridge design, the

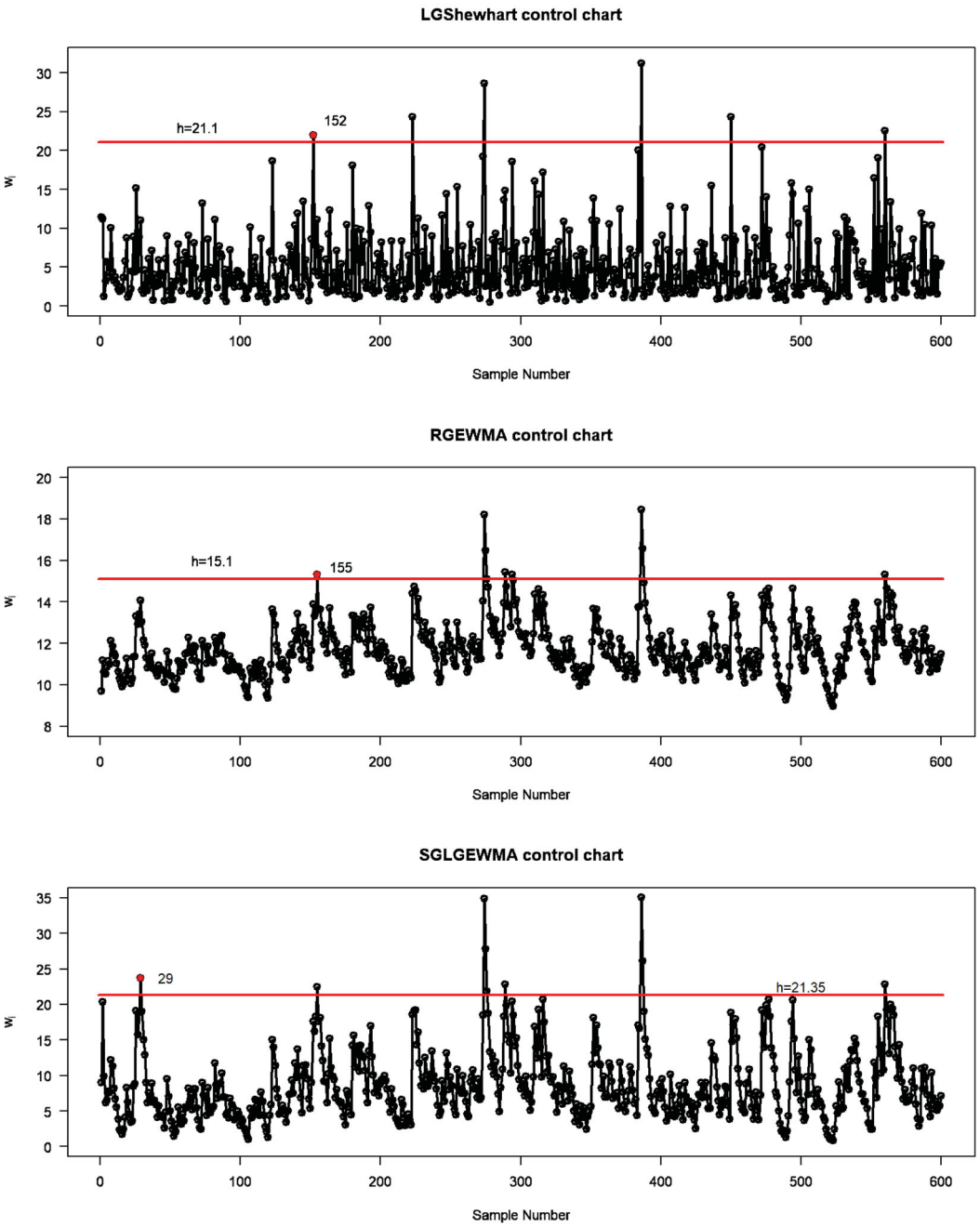

Figure 11. The control charts detection of grinding process data.

proposed control chart performs better in monitoring when the dimension increases. In the sensitivity analysis, the effects of the penalty term tuning parameters λ_1, λ_2 and the smoothing parameter ρ on the monitoring performance of the control chart were investigated. It was found that a smaller smoothing parameter can better monitor small shifts but may weaken the monitoring of large shifts. In the case study, the effectiveness of the proposed control chart

is validated through an example of the semiconductor wafer grinding process, and compared with two other control charts. The results demonstrated that the proposed control chart has better monitoring performance and issues alarms more quickly.

7.2. Future prospects

Since the Euclidean space projections in the proposed control chart are all based on the IC data from Phase I, although the control charts provide better monitoring performance as the dimension increases, sufficient data are still required to ensure that the collected data adequately represent the overall distribution, thereby achieving stability and accuracy. How to effectively monitor a small amount of data, or even data volume less than the dimension, is a topic worthy of further research.

Additionally, to obtain a full-rank sparse estimate of the covariance matrix after sample projection, we employ the ADMM algorithm. While effective, this algorithm has high time complexity and lacks an explicit solution like that of Ridge penalty-based methods, resulting in longer code execution times. Developing a more efficient algorithm may be a worthwhile research direction.

The proposed control chart performs better in Scenario I and Scenario III under Euclidean distance, but its performance under Scenario II is generally average. It may be worth exploring optimizations to the control chart or using control charts with different structures to monitor this type of shift.

Disclosure statement

No potential conflict of interest was reported by the author(s).

Funding

This research was Sponsored by the National Natural Science Foundation of China [grant number 12571305] and the Natural Science Foundation of Shanghai [grant number 25ZR1401113].

ORCID

Chunjie Wu http://orcid.org/0000-0003-2990-9747

References

Adegoke, N. A., Ajadi, J. O., Mukherjee, A., & Abbasi, S. A. (2022). Nonparametric multivariate covariance chart for monitoring individual observations. *Computers & Industrial Engineering*, *167*, Article 108025. https://doi.org/10.1016/j.cie.2022.108025

Ajadi, J. O., Zwetsloot, I. M., & Tsui, K. L. (2021). A new robust multivariate EWMA dispersion control chart for individual observations. *Mathematics*, *9*(9), 1038. https://doi.org/10.3390/math9091038

Alt, F. B. (1984). Multivariate quality control. In S. Kotz, N. L. Johnsonand & C. B. Read (Eds.), *The Encyclopedia of Statistical Sciences* (pp. 110–122). John Wiley.

Boyd, S., Parikh, N., Chu, E., Peleato, B., & Eckstein, J. (2011). Distributed optimization and statistical learning via the alternating direction method of multipliers. *Foundations and Trends® in Machine Learning*, *3*(1), 1–122.

Chakraborty, N., & Finkelstein, M. (2024). Distribution-free multivariate process monitoring: A rank-energy statistic-based approach. *Quality and Reliability Engineering International*, *40*(7), 4068–4087. https://doi.org/10.1002/qre.v40.7

Chowdhury, S., Mukherjee, A., & Chakraborti, S. (2014). A new distribution-free control chart for joint monitoring of unknown location and scale parameters of continuous distributions. *Quality and Reliability Engineering International*, *30*(2), 191–204. https://doi.org/10.1002/qre.v30.2

Danaher, P., Wang, P., & Witten, D. M. (2014). The joint graphical Lasso for inverse covariance estimation across multiple classes. *Journal of the Royal Statistical Society Series B: Statistical Methodology*, *76*(2), 373–397. https://doi.org/10.1111/rssb.12033

Friedman, J., Hastie, T., & Tibshirani, R. (2008). Sparse inverse covariance estimation with the graphical Lasso. *Biostatistics (Oxford, England)*, *9*(3), 432–441. https://doi.org/10.1093/biostatistics/kxm045

Guo, J., Levina, E., Michailidis, G., & Zhu, J. (2011). Joint estimation of multiple graphical models. *Biometrika*, *98*(1), 1–15. https://doi.org/10.1093/biomet/asq060

Hawkins, D. M., & Maboudou-Tchao, E. M. (2008). Multivariate exponentially weighted moving covariance matrix. *Technometrics*, *50*(2), 155–166. https://doi.org/10.1198/004017008000000163

Hoefling, H. (2010). A path algorithm for the fused Lasso signal approximator. *Journal of Computational and Graphical Statistics*, *19*(4), 984–1006. https://doi.org/10.1198/jcgs.2010.09208

Hotelling, H. (1947). Multivariate quality controlillustrated by the air testing of sample bombsights. In C. Eisenhart, M. W. Hastayand & W. A. Wallis (Eds.), *Techniques of statistical analysis* (pp. 111–184). McGraw-Hill.

Huwang, L., Yeh, A. B., & Wu, C. W. (2007). Monitoring multivariate process variability for individual observations. *Journal of Quality Technology*, *39*(3), 258–278. https://doi.org/10.1080/00224065.2007.11917692

Kim, J., Abdella, G. M., Kim, S., Al-Khalifa, K. N., & Hamouda, A. M. (2019). Control charts for variability monitoring in high-dimensional processes. *Computers & Industrial Engineering*, *130*, 309–316. https://doi.org/10.1016/j.cie.2019.02.012

Li, J., Zhang, X., & Jeske, D. R. (2013). Nonparametric multivariate CUSUM control charts for location and scale changes. *Journal of Nonparametric Statistics*, *25*(1), 1–20. https://doi.org/10.1080/10485252.2012.726992

Li, S., Hsu, L., Peng, J., & Wang, P. (2013). Bootstrap inference for network construction with an application to a breast cancer microarray study. *The Annals of Applied Statistics*, *7*(1), 391–417. https://doi.org/10.1214/12-AOAS589

Liang, W., Xiang, D., Pu, X., Li, Y., & Jin, L. (2019). A robust multivariate sign control chart for detecting shifts in covariance matrix under the elliptical directions distributions. *Quality Technology & Quantitative Management*, *16*(1), 113–127. https://doi.org/10.1080/16843703.2017.1372852

Liu, R. Y. (1995). Control charts for multivariate processes. *Journal of the American Statistical Association*, *90*(432), 1380–1387. https://doi.org/10.1080/01621459.1995.10476643

Lowry, C. A., Woodall, W. H., Champ, C. W., & Rigdon, S. E. (1992). A multivariate exponentially weighted moving average control chart. *Technometrics*, *34*(1), 46–53. https://doi.org/10.2307/1269551

Lucas, J. M., & Saccucci, M. S. (1990). Exponentially weighted moving average control schemes: Properties and enhancements. *Technometrics*, *32*(1), 1–12. https://doi.org/10.1080/00401706.1990.10484583

Maboudou-Tchao, E. M., & Agboto, V. (2013). Monitoring the covariance matrix with fewer observations than variables. *Computational Statistics & Data Analysis*, *64*, 99–112. https://doi.org/10.1016/j.csda.2013.02.028

Maboudou-Tchao, E. M., & Diawara, N. (2013). A Lasso chart for monitoring the covariance matrix. *Quality Technology & Quantitative Management*, *10*(1), 95–114. https://doi.org/10.1080/16843703.2013.11673310

Meinshausen, N., & Bühlmann, P. (2010). Stability selection. *Journal of the Royal Statistical Society Series B: Statistical Methodology*, *72*(4), 417–473. https://doi.org/10.1111/j.1467-9868.2010.00740.x

Montgomery, D. C., & Wadsworth, H. (1972). Some techniques for multivariate quality control applications. In *ASQC Technical Conference Transactions* (Vol. 26, pp. 427–435).

Mukherjee, A., & Chakraborti, S. (2012). A distribution-free control chart for the joint monitoring of location and scale. *Quality and Reliability Engineering International*, *28*(3), 335–352. https://doi.org/10.1002/qre.v28.3

Reynolds Jr, M. R., & Cho, G. Y. (2006). Multivariate control charts for monitoring the mean vector and covariance matrix. *Journal of Quality Technology*, *38*(3), 230–253. https://doi.org/10.1080/00224065.2006.11918612

Song, Z., Mukherjee, A., & Zhang, J. (2021). Some robust approaches based on copula for monitoring bivariate processes and component-wise assessment. *European Journal of Operational Research*, *289*(1), 177–196. https://doi.org/10.1016/j.ejor.2020.07.016

Woodall, W. H., & Ncube, M. M. (1985). Multivariate CUSUM quality-control procedures. *Technometrics*, *27*(3), 285–292. https://doi.org/10.1080/00401706.1985.10488053

Xu, F., & Deng, X. (2023). Joint diagnosis of process mean vector and covariance matrix for multivariate statistical process control. *Computers & Industrial Engineering*, *179*, Article 109222. https://doi.org/10.1016/j.cie.2023.109222

Yeh, A. B., Huwang, L., & C. W. Wu (2005). A multivariate EWMA control chart for monitoring process variability with individual observations. *IIE Transactions*, *37*(11), 1023–1035. https://doi.org/10.1080/07408170500232263

Yeh, A. B., Li, B., & Wang, K. (2012). Monitoring multivariate process variability with individual observations via penalised likelihood estimation. *International Journal of Production Research*, *50*(22), 6624–6638. https://doi.org/10.1080/00207543.2012.676684

Zhang, G., & Chang, S. I. (2008). Multivariate EWMA control charts using individual observations for process mean and variance monitoring and diagnosis. *International Journal of Production Research*, *46*(24), 6855–6881. https://doi.org/10.1080/00207540701197028

Zhang, J., Li, Z., & Wang, Z. (2010). A multivariate control chart for simultaneously monitoring process mean and variability. *Computational Statistics & Data Analysis*, *54*(10), 2244–2252. https://doi.org/10.1016/j.csda.2010.03.027

Zou, C., Wang, Z., & Tsung, F. (2012). A spatial rank-based multivariate EWMA control chart. *Naval Research Logistics (NRL)*, *59*(2), 91–110. https://doi.org/10.1002/nav.v59.2

Appendix. Three different OC scenarios

(1) Scenario I: Variance shift

$$\Sigma_{\text{OC\_I}} = (1+\delta)I_p = \begin{pmatrix} 1+\delta & 0 & 0 & \cdots & 0 \\ 0 & 1+\delta & 0 & \cdots & 0 \\ 0 & 0 & 1+\delta & \cdots & 0 \\ \vdots & \vdots & \vdots & \ddots & \vdots \\ 0 & 0 & 0 & \cdots & 1+\delta \end{pmatrix}_{p\times p}.$$

(2) Scenario II: Covariance shift

- When $p = 2$,

$$\Sigma_{\text{OC\_II}} = \begin{pmatrix} 1 & \delta \\ \delta & 1 \end{pmatrix}.$$

- When $p > 2$,

$$\Sigma_{\text{OC\_II}} = \begin{pmatrix} 1 & \delta & \delta & 0 & \cdots & \delta & 0 \\ \delta & 1 & \delta & 0 & \cdots & \delta & 0 \\ \delta & \delta & 1 & 0 & \cdots & \delta & 0 \\ 0 & 0 & 0 & 1 & \cdots & 0 & 0 \\ \vdots & \vdots & \vdots & \vdots & \ddots & \vdots & 0 \\ \delta & \delta & \delta & 0 & \cdots & 1 & 0 \\ 0 & 0 & 0 & 0 & \cdots & 0 & 1 \end{pmatrix}_{p\times p}.$$

(3) Scenario III: Both variance and covariance shift

- When $p = 2$,

$$\Sigma_{\text{OC\_III}} = \begin{pmatrix} 1+\delta & \delta \\ \delta & 1+\delta \end{pmatrix}.$$

- When $p > 2$,

$$\Sigma_{\text{OC\_III}} = \begin{pmatrix} 1+\delta & \delta & \delta & 0 & \cdots & \delta & 0 \\ \delta & 1+\delta & \delta & 0 & \cdots & \delta & 0 \\ \delta & \delta & 1+\delta & 0 & \cdots & \delta & 0 \\ 0 & 0 & 0 & 1+\delta & \cdots & 0 & 0 \\ \vdots & \vdots & \vdots & \vdots & \ddots & \vdots & 0 \\ \delta & \delta & \delta & 0 & \cdots & 1+\delta & 0 \\ 0 & 0 & 0 & 0 & \cdots & 0 & 1+\delta \end{pmatrix}_{p\times p}.$$